ABSTRACT

SPECTROSCOPY IN THE TITANIUM ISOTOPES
VIA (p,d) AND (p,t) REACTIONS

by Phillip James Plauger

Deuteron angular distributions from $^{48}Ti(p,d)^{47}Ti$ were measured at incident proton energies of 24.80, 29.82, 35.15, 39.97 and 45.05 MeV to detect the presence of any energy dependence in various methods of extracting spectroscopic factors. Using optical parameters obtained from the literature, distorted wave Born approximation calculations were performed with the Oak Ridge code JULIE for the principal L_n= 1, 2 and 3 transitions observed. In all cases, significantly better agreement with the data was obtained in the zero-range approximation by using a lower integration cutoff at the nuclear surface. The variation of spectroscopic factors with cutoff radius also exhibited a plateau at the nuclear surface; however energy dependence of extracted spectroscopic factors was still present. The best agreement was obtained by applying finite range and non-locality corrections to the form factors used by JULIE. No integration cutoffs were required and energy dependence was removed.

Partial angular distributions from $^{46}Ti(p,d)^{45}Ti$ at 34.78 MeV and $^{50}Ti(p,d)^{49}Ti$ at 45.05 MeV were also measured.

Using the prescription obtained from the energy dependence study, spectroscopic factors were obtained for transitions to $^{45,47,49}Ti$.

The reactions $^{46,48,50}Ti(p,t)^{44,46,48}Ti$ were performed from 25 to 45 MeV in an attempt to excite T= T_z+2 analog states. Only the T= 2 state at 9.31 MeV excitation in ^{44}Ti was observed. The ground state Q-value for $^{46}Ti(p,t)^{44}Ti$ was found to be -14.246(0.011) MeV.

SPECTROSCOPY IN THE TITANIUM ISOTOPES VIA (p,d) AND (p,t) REACTIONS

by

Phillip James Plauger

A THESIS

Submitted to

Michigan State University

in partial fulfillment of the requirements

for the degree of

DOCTOR OF PHILOSOPHY

Department of Physics

1969

ACKNOWLEDGMENTS

While it is a convenient fiction that a doctoral thesis is the work of one person, in a cyclotron laboratory this is far from the truth. In any endeavor, the assistance of Professor Henry Blosser, Harold Hilbert, N. Mercer and their technical staffs is required throughout. I gratefully acknowledge receiving their help in many ways. Others have contributed their time and talents to this thesis in a more specific fashion:

I wish to thank Ivan Proctor for the use of the detector bench he developed and built, and Douglas Bayer for the extensive use of his program TOOTSIE.

Fred Trentelman and Larry Learn helped me acquire the bulk of the data used in this study. For both their help in operating the cyclotron and late-night company I am grateful.

Particular thanks goes to Bryan Horning for the many hours he spent reducing this data. And to Mrs. Karen Fox for preparing the illustrations.

Much of my understanding of optical model and distorted wave calculations I owe to Dr. Barry Preedom. His advice and suggestions proved invaluable on more than one occasion. Many conversations with Professor Rubby Sherr have taught me much about nuclear spectroscopy and stimulated much deep thought.

Finally and most important, I wish to thank Professor Edwin Kashy for his extensive assistance throughout this thesis, and for his sound guidance throughout my collegiate career.

TABLE OF CONTENTS

LIST OF TABLES

LIST OF FIGURES

1. INTRODUCTION

The study of (p,d) reactions in the titanium isotopes provides useful information about both the reaction mechanism and the nuclei themselves. Stable titanium nuclei have Z= 22, N= 24 - 28, and so each can be treated as a ^{40}Ca core plus particles mainly in the $1f_{7/2}$ shell. The (p,d) reaction consists principally of picking up a neutron from one of the outer shells of the target, with a minimum of configuration rearrangement. Therefore one would expect to observe at least one strong L= 3 transition, corresponding to the pickup of a $1f_{7/2}$ neutron, and some L= 1 strength due to the admixture of the next higher subshell, $2p_{3/2}$. Even L transfers, pickup from the filled 2s-1d shell, are also expected.

The strength of these transfer reactions is a very direct measure of the overlap of the final state and target ground state wave functions. Since the shape of the angular distribution strongly depends on the L-transfer, the principal transitions can be sorted fairly well according to the orbital from which they originate. Given a theory of the reaction mechanism, one can then determine the occupation probabilities of the various shell model orbitals. Such a theory is the distorted wave Born approximation, embodied in the Oak Ridge computer code JULIE (Ba 62). The transition strengths measured by comparing experimental cross-sections

to DWBA predictions are called spectroscopic factors.

Consistency checks exist for these factors. Since the sum of all spectroscopic factors for picking up a neutron from a shell gives its total occupancy, the sum has a rigorous upper bound. One expects inner shells to be essentially filled, closely defining their sums. Still other "sum rules" exist for other constraints, as will be seen later. There exist also the calculations, by McCullen, Bayman and Zamick (Mc 64), of the wave functions of $(1f_{7/2})^n$ configuration states. These provide a basis for predicting spectroscopic factors and other nuclear properties of the titanium isotopes.

Such considerations raised questions about the results obtained from $^{46-50}Ti(p,d)^{44-48}Ti$ studies at 17.5 MeV by Kashy and Conlon (Ka 64). DWBA calculations using the zero-range approximation consistently predicted less than one neutron in the $1d_{3/2}$ shell and, in ^{48}Ti, nearly two neutrons in the $2p_{3/2}$ shell.

Still other difficulties were reported by Sherr, et al. (Sh 65) in a study performed at 28 MeV which included $^{48,50}Ti(p,d)^{47,49}Ti$. These experiments also excited high-lying isobaric analog states - states having a total isotopic spin one greater than the low-lying states and configurations analogous to the low-lying states in their scandium isobars. Applying sum rules to the different isospin states, developed by French and Macfarlane (Fr 61), Sherr et al. were able to study the dependence of DWBA predictions on reaction Q-value.

Using normal procedures they found too large a Q dependence for L= 3 transfers and were led to an "effective binding" prescription to improve agreement with the sum rules. This procedure has since been shown to be theoretically unsound (Pi 65).

Some hope for improving this state of affairs was raised by Snelgrove and Kashy (Sn 69) in a study of $^{16}O(p,d)^{15}O$ over an energy range of 21 to 45 MeV. They discovered strong energy dependence in the extraction of spectroscopic factors up to a deuteron exit energy of about 20 MeV. Consequently, it was decided to extend this energy dependence investigation to ^{48}Ti in the hope of better understanding the mechanics of extracting spectroscopic factors. At the same time $^{46,50}Ti(p,d)^{45,49}Ti$ measurements were made, each at one energy, to explore the systematics of the (p,d) reaction across the titanium isotopes and to apply the knowledge gained from the energy investigation.

Since data for these studies were acquired on-line by the laboratory's SDS Sigma 7 computer, it was an easy matter to retain spectra of the tritons detected during the (p,d) experiments. Thus it was possible to obtain additional information on isobaric analog states, which have attracted considerable attention of late, including analogs to states in calcium. Supplemented by several runs devoted to obtaining good triton statistics, the (p,t) data also permitted a determination of many of the excited states in ^{44}Ti.

2. NUCLEAR THEORY

2.1 The Shell Model with Residual Interactions

The nuclear shell model (de 63) forms the basis for nearly all calculations in the titanium mass region. In its simplest form, it describes the nucleus as a collection of neutrons and protons in different orbitals, each nucleon interacting with the others only through an average potential well formed by the remaining particles. Figure 2.1 shows such a well, of the usual Woods-Saxon form, and the calculated spectrum of stationary neutron single particle states. These orbitals are subsequently split by a strong spin-orbit interaction to give the major shell groupings and "magic" occupation numbers 2, 8, 20, 28. . . shown. The well parameters and spin-orbit strength used are fairly realistic (Be 64) for A= 48 nuclei.

To pickup a neutron from the highest occupied shell, $1f_{7/2}$, one must provide the separation energy S= 13 MeV, approximately. Since 2.22 MeV is liberated on forming a deuteron, the mass energy released in a (p,d) reaction would be Q= 2.22 - S, or about -11 MeV. Pickup from the 2s-1d shell would then lead to three excited states between seven and ten MeV, not including the Coulomb analog transitions also expected. Unfortunately, while the predicted ground state

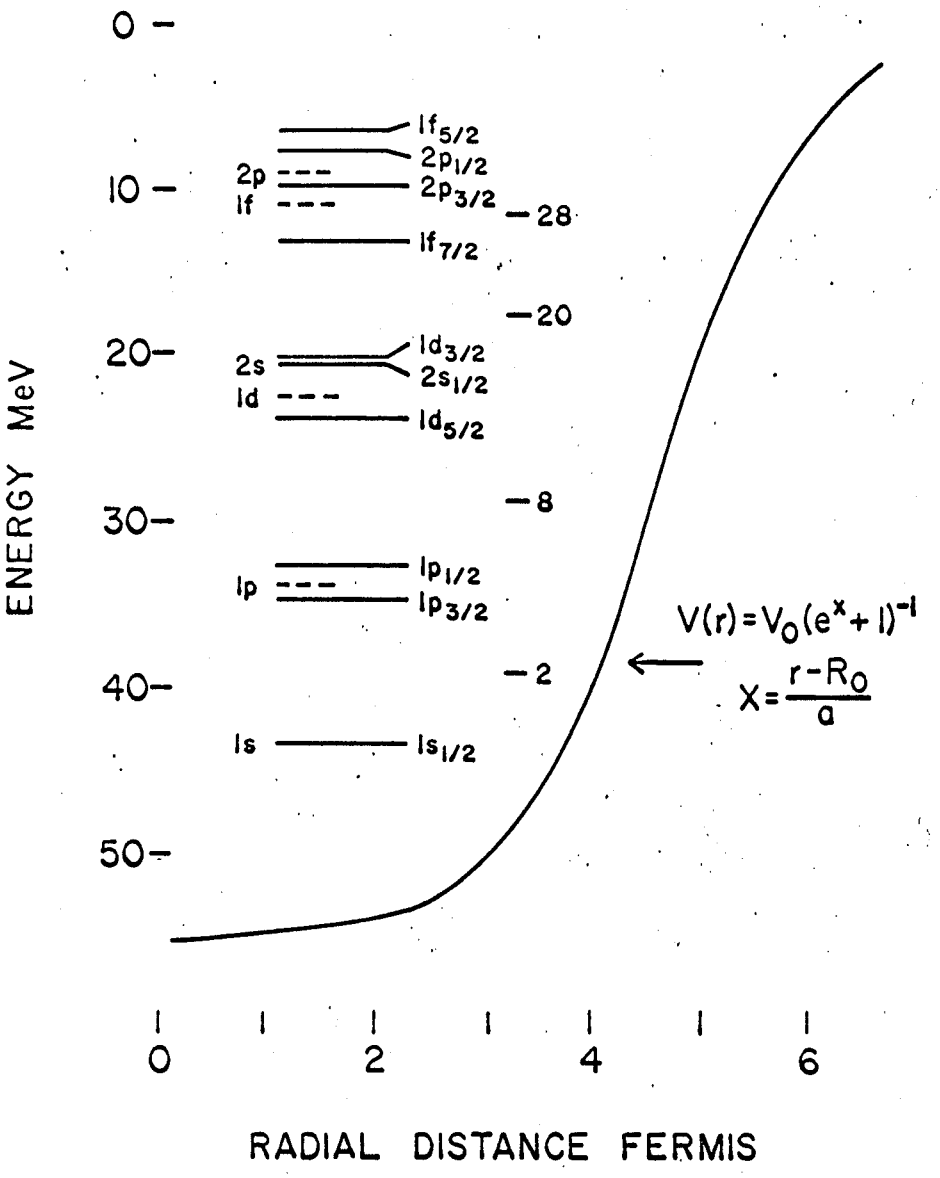

Figure 2.1 Neutron single particle energy levels.

Q value is essentially correct, many more than three excited states are observed below 15 MeV in (p,d) reactions.

Clearly there must be residual interactions between the nucleons which split the single particle levels into many states. One approach to estimating this effect is that taken by McCullen, Bayman and Zamick (Mc 64). Confining their attention to pure $(1f_{7/2})^n$ configurations, they obtained empirical two-body interaction energies from the spectrum of ^{42}Sc. Since this nucleus consists of two non-identical $1f_{7/2}$ nucleons outside a closed core, one expects eight levels with total spins J= 0 - 7, giving the interaction energy differences. These differences are sufficient to determine the matrix elements of the residual interactions between all possible orthogonal wave functions of a given J. Diagonalizing this matrix gives the physical wave functions of spin J and their relative energies.

These wave functions are tabulated (Mc 64a). As an example of the versatility of even pure $(1f_{7/2})^n$ configurations, the spectrum predicted for ^{47}Ti consists of 133 levels below 15 MeV. Seventeen of these are J= 7/2, easily reachable by an L= 3 (p,d) transition. Splitting of the "hole" states, due to 2s-1d pickup, is of course not computed in the MBZ scheme. Nor is pickup from shells above $1f_{7/2}$ considered, since no valence nucleons are assumed to be there. But the calculations do include the wave functions of the targets used, and of the principal levels

reached by L= 3 transfers. Thus it is possible to compute several important spectroscopic factors.

2.2 Spectroscopic Factors and Sum Rules

A direct reaction can be characterized by the fact that only a few internal degrees of freedom of the interacting system are excited (Ba 62). Since there is no intermediate stage of compound nucleus formation, the (p,d) interaction is dominated by the overlap of the initial and final nuclear states. Thus, in the absence of polarization the (p,d) differential cross-section can be written (Mc 64, Ba 62)

$$\frac{d\sigma}{d\Omega}_{Lsj} = \frac{3}{2} S \sigma_{Lsj} \qquad (2.1)$$

where S is the spectroscopic factor. The 3/2 arises from summing over the spin states of the deuteron and averaging over those of the proton. Sigma is the mechanism-dependent cross-section for transferring a given Lsj, assuming one particle available for pickup. It is this function that is computed in the distorted wave Born approximation by the code JULIE.

The spectroscopic factor contains the overlap information. Thus it can be written (Mc 64)

$$S = N \left(\langle \psi_f + n \mid \psi_i \rangle \right)^2 \qquad (2.2)$$

where N is the number of neutrons in the shell from which pickup occurs, the ket is the target wave function and the bra is the final state wave function coupled to a neutron in the picked-up orbital. A straightforward example is

$^{50}Ti(p,d)^{49}Ti(G.S.)$. MBZ naturally predicts $(j_p\ j_n\ J)$= (0 0 0) for the target wave function, since the neutron shell must be closed; and N is eight. From the tables (Mc 64a)

$$(^{49}Ti\ G.S.) = -0.9136(0\ 7/2\ 7/2) + 0.4058(2\ 7/2\ 7/2) + 0.0196(4\ 7/2\ 7/2) - 0.0146(6\ 7/2\ 7/2) \quad (2.3)$$

There is only one way to add a neutron to this wave function, and only the first term contributes to the inner product. Thus S= 6.68 in this case. Table 2.1 shows the spectroscopic factors for the principal predicted transitions from even-A titanium targets.

Table 2.1 Predicted energies and spectroscopic factors for $1f_{7/2}$ pickup.

$^{46}Ti(p,d)^{45}Ti$			$^{48}Ti(p,d)^{47}Ti$			$^{50}Ti(p,d)^{49}Ti$		
Excitation	T	S	Excitation	T	S	Excitation	T	S
0.28 MeV	1/2	3.10	0 MeV	3/2	4.77	0 MeV	5/2	6.68
3.87	1/2	0.17	2.50	3/2	0.14	2.53	5/2	0.59
4.42	3/2	0.67	2.87	3/2	0.55	4.86	5/2	0.44
4.75	1/2	0.05	4.13	3/2	0.01	8.40	7/2	0.29
			4.55	3/2	0.05			
			5.51	3/2	0.04			
			6.11	3/2	0.02			
			6.46	3/2	0.02			
			6.48	5/2	0.40			

Basic sum rules follow directly from Equation 2.2 and the discussion of the previous section. Adding up the squared amplitudes of all transitions of a given Lsj is merely a way of regrouping the single particle strength split by residual interactions. Since in the simple model the initial and final states of a (p,d) reaction would overlap completely, the single particle spectroscopic factor

is just the number of particles in the orbital.

The sum rules derived by French and Macfarlane (Fr 61) apply to transitions to the higher T, or analog, states of the residual nucleus, which are also isotopically allowed in (p,d). Thus

$$S = P/(2T + 1) \qquad (2.4)$$

where S is the spectroscopic factor (or sum if the strength is split) for a transition of given Lsj to an analog state, P is the number of protons in the target Lsj orbital and T is the total isospin of the target. Table 2.2 gives the predicted sums for pickup from the outer orbitals of the even titanium isotopes.

Table 2.2 Sum rule predictions for neutron pickup from valence orbitals.

Target	$1f_{7/2}$		$1d_{3/2}$		$2s_{1/2}$	
	T-lower	T-upper	T-lower	T-upper	T-lower	T-upper
^{46}Ti	3.33	0.67	2.67	1.33	1.33	0.67
^{48}Ti	5.60	0.40	3.20	0.80	1.60	0.40
^{50}Ti	7.71	0.29	3.43	0.57	1.71	0.29

One can obtain the results of French and Macfarlane in a straightforward manner in the case of analog hole states. As an example, consider ^{46}Ti(p,d)^{45}Ti(T= 3/2 J= 3/2+). Using the notation (# of $1f_{7/2}$ protons, # of $1f_{7/2}$ neutrons) (# of $1d_{3/2}$ protons, # of $1d_{3/2}$ neutrons), one can express the corresponding hole state in ^{45}Sc as (2 4)(3 4), obtained by promoting a proton from the ground state configuration

(1 4)(4 4). Applying the T^- ladder operator should leave T= 3/2 and change scandium into titanium. Thus

$$T^-(2\ 4)(3\ 4) = (2/3)^{1/2}\ (3\ 3)(3\ 4) + (1/3)^{1/2}\ (2\ 4)(4\ 3) \qquad (2.5)$$

where the wave function has been normalized. On coupling a $d_{3/2}$ neutron, the first term drops out and the second becomes just the target ground state wave function. Thus S= 4(1/3) from Equation 2.2, in agreement with French and Macfarlane.

2.3 The Distorted Wave Born Approximation

The cross-sections defined in Equation 2.1 were computed on the SDS Sigma 7 by the distorted wave Born approximation code JULIE (Ba 62, Sa 64). In the plane wave Born approximation, one treats all scattering as a first order perturbation; i.e. the initial and final states are free particle wave functions, and the interaction potential is the perturbation that causes the transition. It is far more realistic, however, to describe the relative motion of the interacting bodies before and after the transition by waves distorted by an optical potential. These potentials are chosen to closely approximate elastic scattering data for the entrance and exit channels.

Using the reaction notation A(a,b)B, the differential cross-section is written (Ba 62)

$$\frac{d\sigma}{d\Omega} = \frac{\mu_a \mu_b}{(2\pi\hbar^2)^2} \frac{k_b}{k_a} \frac{\sum_{M_A M_B m_a m_b} |T|^2}{(2J_A+1)(2s_a+1)} \qquad (2.6)$$

where the mus are reduced masses and the k's are momenta. The transition amplitude T is of the form (Sa 64)

$$T = \int d\vec{r}_{aA} \int d\vec{r}_{bB}\, \phi^{(-)*}_{bB}(\vec{k}_b, \vec{r}_{bB}) \langle bB|V|aA\rangle \phi^{(+)}(\vec{k}_a, \vec{r}_{aA}) \quad (2.7)$$

where the phis are the distorted waves, satisfying incoming (-) and outgoing (+) boundary conditions. The matrix element describes the effective interaction taken between the internal states of the colliding pairs. In the case of (p,d) it is assumed that the proton-neutron interaction V_{pn} causes the transition to occur. Thus the matrix element can be written

$$\langle bB|V|aA\rangle = \langle B|A\rangle \langle d|V_{pn}|p\rangle \quad (2.8)$$

where the nuclear overlap is usually taken to be the wave function of the transferred neutron.

Since Equation 2.7 involves a six-dimensional integral which is extremely difficult to evaluate numerically, the zero-range approximation is usually introduced. This is accomplished by replacing the p-n interaction matrix element by a constant, D_o, times a delta function in the separation of the proton and neutron in the deuteron. Aside from collapsing the integral to three dimensions, this approximation invokes several physical assumptions. Principally, it means that the deuteron is created at the same point at which the proton is absorbed. Also, it ignores any tensor forces in the p-n interaction and neglects all but the S-wave of the deuteron internal state function. These assumptions are best met in the case of low momentum transfers, and become increas-

ingly worse as the amount transferred increases (Sa 64).

The effective interaction is expressed in terms of the Lsj transferred and the distorted waves are expanded into a sum of partial waves of different L. The computer code JULIE calculates the necessary transition amplitudes on this basis and outputs the (p,d) cross-section in millibarns per steradian. Because the code uses a factor D_o computed on the basis of a delta-function bound deuteron instead of the Hulthen wave function, the cross-section computed by JULIE must be multiplied by 1.5 to give the sigma used in Equation 2.1 (Ba 62).

Calculations involving finite range (Au 64) and non-local (Au 65) interactions have been investigated. Both tend to damp the contribution of the nuclear interior, which is known to be necessary to improve agreement with data. Since finite range calculations are difficult and time comsuming, the "local energy approximation" has been exploited to approximate finite range (Be 64a, Bu 64) and non-local (Pe 64) effects. This results in a radial damping function which modifies the neutron bound-state wave function used in the zero-range calculation. Comparison between such calculations and full six-dimensional integrations have been made (Di 65) and are found to agree reasonably well. Finite range and non-local (FRNL) damping factors used in this study were computed on the Sigma 7 by the code WAVDAM (Sa 69).

3. EXPERIMENTAL PROCEDURE

3.1 Beam Production and Handling

Proton beams for these experiments were accelerated in the Michigan State University sector focussed cyclotron (Bl 66). Between 70 and 100 per cent of the internal H^+ beam was extracted via an electrostatic deflector and magnetic channel. Figure 3.1 shows a floor plan of the cyclotron experimental area and the beam line used.

The transport system (Ma 67) focussed the extracted proton beam from the cyclotron on slits S1, and subsequent foci were formed at slits S3 and at the center of the 36-inch scattering chamber. The energy analysing system, consisting of 45-degree bending magnets M3 and M4, quadrupoles Q5 and Q6 and sextupoles SX1 and SX2, was designed to give an energy resolution of one part in 1000 for 0.130 inch horizontal slit openings at S1 and S3. In these studies the energy spread in the beam was kept at approximately 25 keV.

Beam divergence was controlled by slits S2, positioned 51.75 inches from S1. A typical opening of 0.40 inch limited beam divergence to +/- 4 mrad. Since the total magnification between S1 and target is just under one, a properly focussed beam could be kept within a 0.1 inch wide

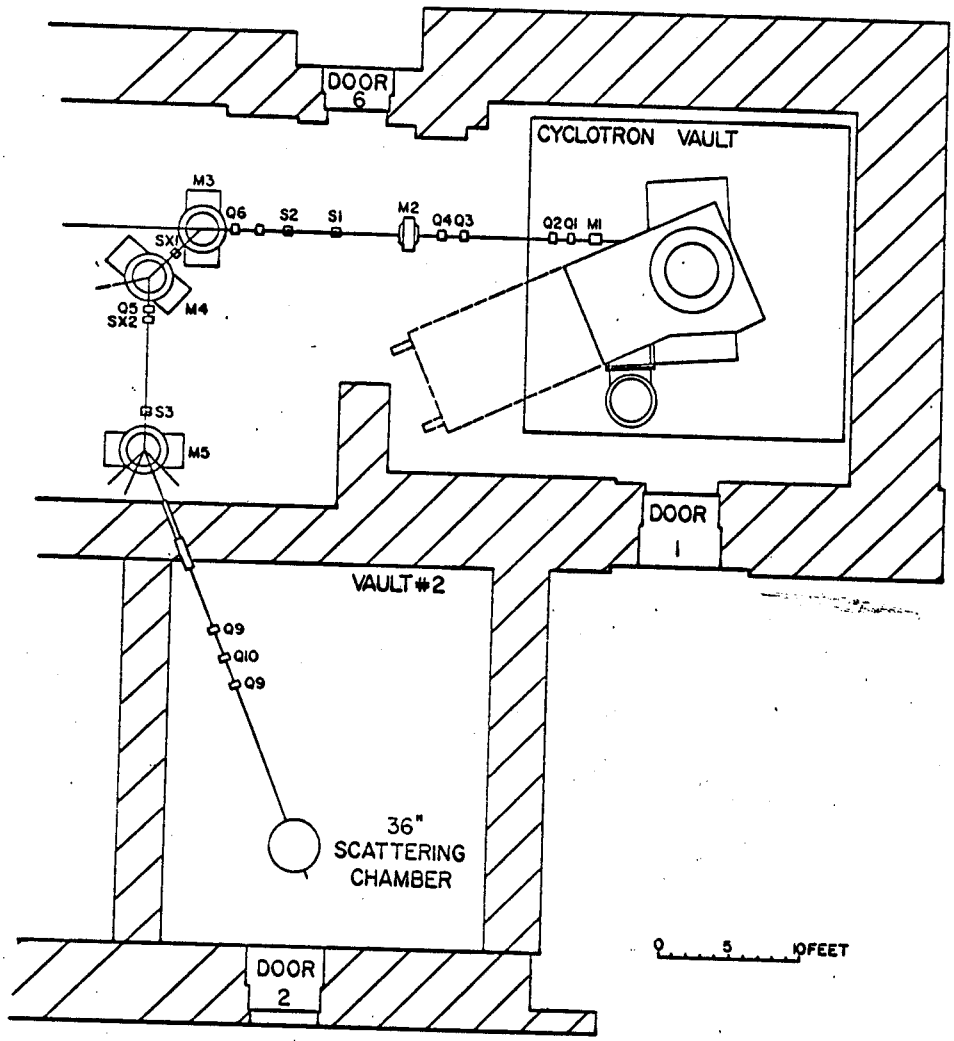

Figure 3.1 Floor plan of cyclotron experimental area.

by 0.15 inch high area on target. Closed circuit television cameras and scintillators at each of the three foci permitted visual alignment of the beam before each run.

Proton energies were determined from nuclear magnetic resonance fluxmeters in the central fields of M3 and M4. These magnets were always set following a standard cycling procedure to insure proper field shape. Energy reproducibility has been estimated at one part in 15000 (Sn 67) and absolute energy at better than one part in 1000, based on the consistent agreement of several recent measurements in the laboratory.

Targets used in these experiments are described in Table 3.1. All targets were cut to approximately one inch squares, weighed and measured before mounting in frames. It is believed that the thicknesses determined are accurate to four per cent.

Table 3.1 Isotopic analysis of targets by atomic per cents.

Target	(mg/cm^2)	^{46}Ti	^{47}Ti	^{48}Ti	^{49}Ti	^{50}Ti
^{46}Ti	1.054	86.1	1.6	10.6	0.8	1.0
^{48}Ti	0.923	0.17	0.2	99.36	0.17	0.11
^{50}Ti	1.090	3.1	2.39	22.8	2.02	69.7

Beam passing through the scattering chamber was collected in a 2.9 inch diameter by 11.5 inch deep Faraday cup. An Elcor A310B current indicator and integrator connected to the cup was used to monitor beam intensity and to measure the total charge passed through the target during a run.

Currents were kept low enough to insure negligible pileup of pulses in the detectors and overall system dead time under four per cent. First order corrections were made to the integrated charge for the observed dead time. Periodic checks of the current integrator during the course of this study showed the absolute calibration to remain within one per cent.

3.2 Particle Detection and Identification

Charged particles scattered from the target were detected in a counter telescope consisting of three commercial silicon surface barrier detectors purchased from Ortec. All were totally depleted and transmission mounted. The front counter, 260 microns thick, provided a "delta-E" signal. The remaining two counters were operated in parallel to provide the 4000 microns of silicon needed to stop the most energetic deuterons of interest and thus produce an "E" signal. The entire telescope was cooled by methanol circulated around a dry ice bath at -78° C.

A tantalum collimator, between 0.050 and 0.090 inch thick depending on beam energy, was mounted in front of the telescope to define the solid angle and angular acceptance. Typical solid angles were on the order of 10^{-4} steradian with an angular acceptance of 0.8 degree. The angle of the detector telescope to the beam was read from a remote digital voltmeter readout which, if care was taken to eliminate

backlash, could be set reproducibly within 0.2 degrees. The zero degree line was optically determined before each run and checked by measuring spectra on both sides of the chamber. These were always found to agree within the limits of angular uncertainty.

Figure 3.2 is a schematic diagram of the detector electronics. The 5 M resistor to ground provided a signal proportional to the sum of the charges deposited in all detectors, and thus proportional to the total energy of a particle stopped in the telescope. This method of "charge summing" eliminates the necessity of closely matching amplifier gains before forming a sum pulse.

The control logic for the experiment is shown in Figure 3.3. The E and delta-E signals are fed into Ortec 440 filter amplifiers where they are double delay line clipped and passed on to Ortec 220 single channel analyzers. A coincidence pulse is formed in an Ortec 409 linear gate and slow coincidence to control input to both analog to digital converters. To keep electronic noise to a minimum, the sum pulse is amplified in a Tennelec TC200, where it also is double delay line clipped. To synchronize with the control logic, the amplified sum pulse is delayed by an Ortec 427 amplifier before passing through the Ortec 426 linear gate.

Particle identification could be performed by plotting delta-E against the total energy pulse. Particles with different Z^2A fall on separate hyperbolic bands. It is easier to distinguish between these bands, however, if E

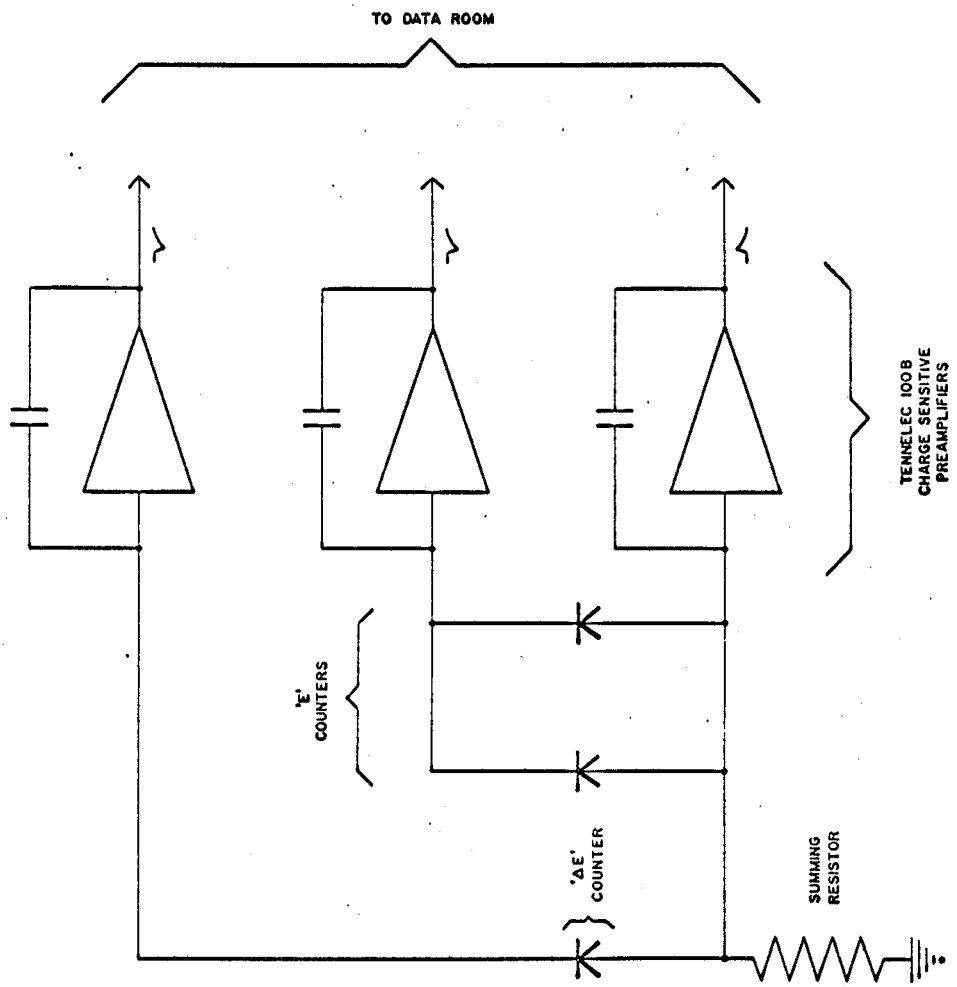

Figure 3.2 Schematic of detector electronics.

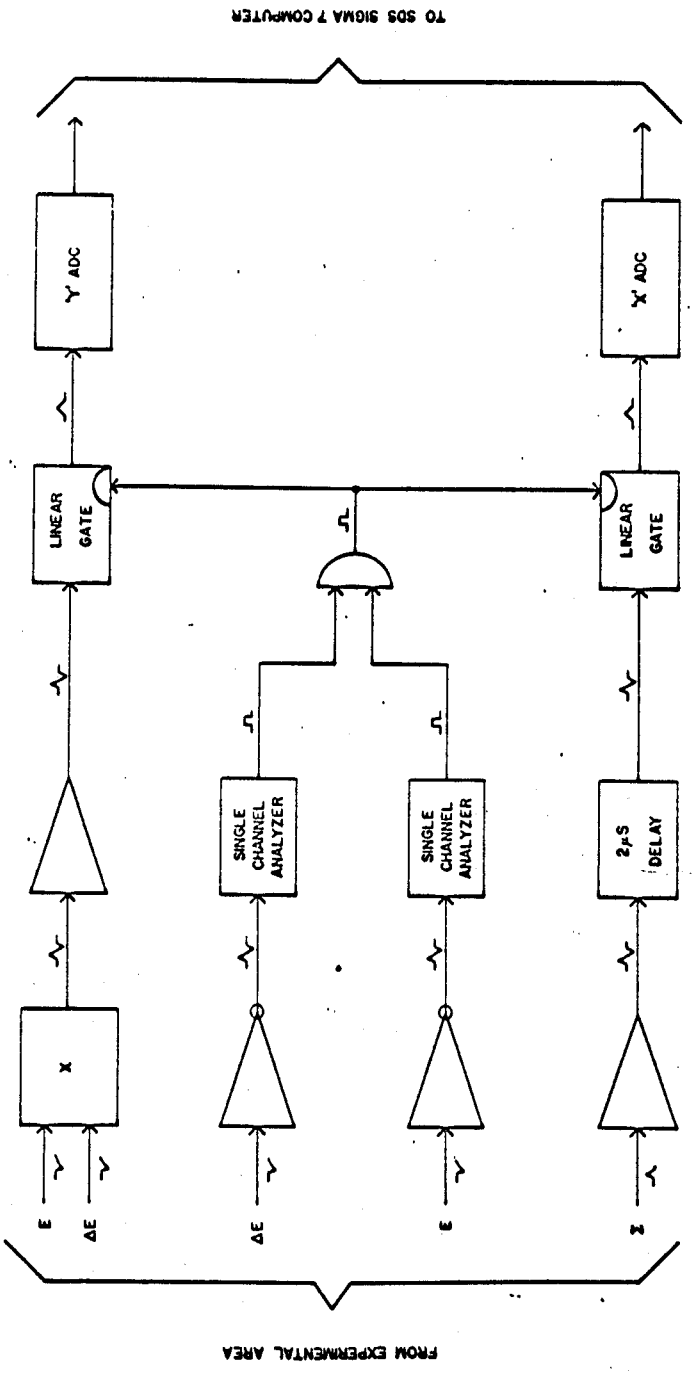

Figure 3.3 Block diagram of experiment control logic.

times delta-E is the ordinate, since the bands thus formed are essentially straight. Thus a field effect transistor pulse multiplier (Mi 63) is used to form this product, which is input to an Ortec 440 and passed through the 409 linear gate.

The gated mass and energy pulses were fed into a pair of Northern Scientific 629 13-bit analog to digital converters under control of the cyclotron laboratory's Scientific Data System Sigma 7 computer. Most of the data in this study was processed under the on-line acquisition code TOOTSIE, written by D. Bayer (Ba 69). Final runs were made using task GEORGE, written by the author (Pl 69) to perform a subset of the TOOTSIE options, operating under the realtime timesharing system JANUS (Ko 68). The latter code is described here.

GEORGE operates in two principal modes. The first, SETUP mode, acquires two parameters and displays them as a 32x128 two-dimensional array. Gate lines can be defined by accepting a series of points on the 2D raster and requesting that a polynomial of given order be fit through them. Each pair of lines defines a band, inside which all events are treated as being the same particle. Once one or more bands are defined, RUN mode is entered to acquire data as singles spectra of different particle types. Figure 3.4 is a flow chart of the routine which processes an event in RUN mode.

Sample values of the gate lines are computed for every

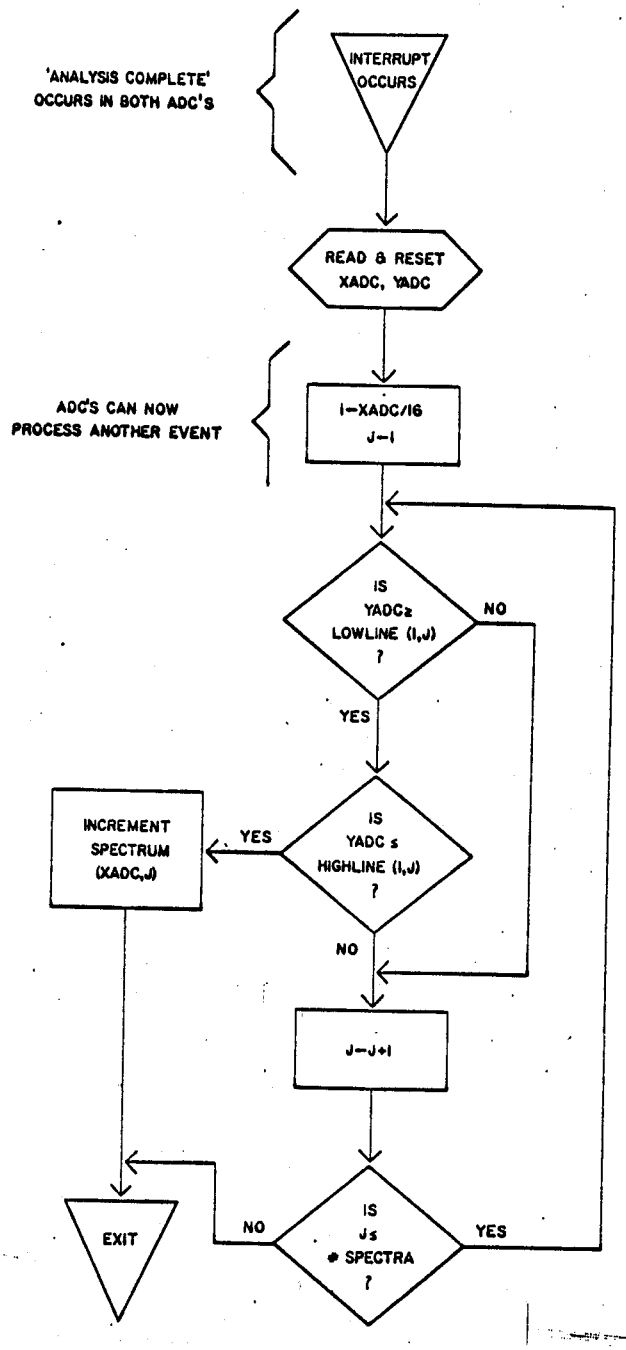

Figure 3.4 Flow chart of data acquisition routine.

16 channels along the abscissa. Thus the Sigma 7 computer is made to act as a large raster of SCA's, each covering a narrow strip of energy. This not only greatly relaxes the requirements on the mass identification parameter, it also permits the simultaneous acquisition of more than one particle spectrum without elaborate routing hardware. In these (p,d) experiments it was common practice to monitor (p,p) and acquire (p,t) spectra at the same time, using three 2048-channel storage areas.

3.3 Error Analysis

Overall energy resolution was between 50 and 60 keV for all data acquired. Table 3.2 lists the major contributions to the resolution at 40 MeV. Electronic noise was measured by injecting pulses into the system at the preamplifier input (with the detectors cooled and connected), and measuring the analyzed peak width. Straggling was estimated for a one mg/cm^2 titanium target from tabulated energy loss data (Wi 66).

Table 3.2 Contributions to energy resolution at 40 MeV.

Source	Contribution
Electronic noise	35 keV
Beam resolution	25
Straggling in target	16
Finite size of collimator	13
Finite size of beam	10
Divergence of beam	8
Added in quadrature	49 keV
Experimental	55

Differential cross section is defined experimentally as the number of product particles scattered into a given solid angle divided by (1) the number of incident particles, (2) the number of scattering centers per unit area and (3) the size of the solid angle. The integrated charge counts the number of protons, since each has a unit of charge. Since a gram-molecular weight contains Avogadro's number of particles, the measured target thickness counts scattering centers. Combining these factors gives

$$\frac{d\sigma}{d\Omega} = 2.659 \times 10^{-4} \, n \, \frac{\sin\theta}{Q} \, \frac{MW}{tf} \, \frac{d^2}{A} \qquad (3.1)$$

where n is the number of events, theta the angle of the target foil to the beam, MW the mean molecular weight of the foil, d the collimator to target distance, Q the integrated charge in microCoulombs, t the foil thickness in mg/cm^2, f the fraction of foil atoms to be considered targets, and A is the area of the collimator in the same units as d. The resulting cross section is in microbarns per steradian (10^{-30} cm^2).

Table 3.3 summarizes the sources of error in determining cross-sections, which combine to give 5.1 per cent. In addition to this systematic error, each measurement has its own statistical error due to fluctuations in counting. Errors in counting are Poisson distributed and so, for a large enough number of counts, A, can be approximated by a normal distribution whose standard deviation is $A^{1/2}$. In general a background, B, is estimated for each deuteron or triton group and assigned an error

equal to its square root. Adding errors in quadrature gives for a net area A-B the statistical error $(A+B)^{1/2}$. Error bars on the data presented in this thesis reflect only this statistical error.

Table 3.3 Contributions to uncertainty in cross-sections.

Source	Contribution
Target thickness	4.0 per cent
Area of collimator	2.5
Target angle (sine)	1.5
Integrated charge	1.0
Collimator to target distance (squared)	1.0
Added in quadrature	5.1 per cent

Calibration points for the energy scale in each run were obtained by (p,d) scattering from 0.00025 inch thick mylar, a plastic containing only carbon, hydrogen and oxygen, and the (p,d) transitions to the ground states of ^{45,49}Ti and to the strong 0.160 MeV state in ^{47}Ti. All of these Q values are well established (Ma 65, Fr 66, En 67) with assigned errors of only a few keV, and provide calibration points bracketing the region of interest in deuteron energy. Gains varied between 15 and 20 keV per channel for different runs. It was found that the ADC zero level changed extensively between spectra, necessitating the use of a calibration peak in each spectrum to define the zero offset. No explanation has been found for this effect. Evidence also exists for gain shifts, mostly small, between runs. These correlate strongly with variations in the building AC line voltage.

Another unfortunate effect was observed arising from the use of two "E" detectors. The inner faces of the counters represented a dead layer approximately 160 keV thick for four MeV deuterons. Thus those particles that stopped in the first counter appeared more energetic, that is at a lower excitation, than was consistent with the more energetic calibration groups. Fortunately the major non-linearities due to this dead layer occurred in the region of interest only at 40 MeV beam energy, and there in a region of excitation containing only weak transitions.

The problems in calibrating the energy scale were reflected in the root mean square deviations of the calibration line fits and in the scatter of measured excitations for the same state from one spectrum to another. RMS deviations were typically eight to 16 keV for the calibrations, and varied from seven to about 25 keV for excitations, increasing with decreasing cross-section. However the presence of small quantities of vacuum pump oil, due to backstreaming from the scattering chamber roughing pump, provided a fortuitous carbon calibration amidst the high-lying titanium levels in several runs. From the jitter in the centroids measured for these small carbon groups, it is estimated that the systematic error in excitation energies is 0.6 per cent. Within these limits, the data in this thesis is in agreement with several earlier studies (Ka 64, Sh 65, Ra 66).

Other measurements (Ro 67, An 69), however, indicate

that the $^{50}Ti(p,d)^{49}Ti$ calibration is low by 1.5 per cent. This disagreement is probably due to the erroneous identification of carbon groups in this study, since the ^{50}Ti foil was exposed the least to pump oil contamination. One of the measurements (Ro 67) also indicates that the energy calibration is 0.5 per cent low for the other two (p,d) reactions studied here. Corrected excitation energies will be presented with the measured values in this thesis.

4. OPTICAL MODEL PARAMETERS

The distorted waves used in code JULIE describe the relative motion of protons elastically scattered from the target and of deuterons elastically scattered from the residual nucleus at the appropriate energies. These waves are calculated using an optical model, where experimental scattering data are used to determine the parameters of the potential. All parameters used in this thesis are taken from the literature, or are determined by averaging over several published sets.

There are several contributions to the optical potentials used. All but the Coulomb term involve either a "volume" Woods-Saxon geometry (see Figure 2.1) or a "surface" term formed by differentiating the volume form. Let

$$f(r,r_o,a)= 1/(\exp(x) + 1) \qquad (4.1)$$

where

$$x= (r - r_o A^{1/3})/a \qquad (4.2)$$

Then the potential used is a sum of:

a real volume term

$$-V\ f(r,r_o,a) \qquad (4.3)$$

an imaginary volume term

$$-i\ W\ f(r,r_{oI},a_I) \qquad (4.4)$$

an imaginary surface term

$$4i\ W_D\ d/dx_I\ f(r,r_{oI},a_I) \qquad (4.5)$$

a Thomas type spin-orbit term

$$(\hbar/mc)^2 V_{so} (1/r) d/dr f(r,r_s,a_s) \underline{L}.\underline{s} \qquad (4.6)$$

where m is the mass of the pion,

and a Coulomb repulsion term

$$ZZ'e^2/r \text{ outside } R_C = r_C A^{1/3} \qquad (4.7)$$

and

$$ZZ'e^2/2r (3 - (r/R_C)^2) \text{ inside.} \qquad (4.8)$$

The imaginary terms account for loss of probability current from the elastic channel due to all other processes.

Proton optical model parameters were obtained from the 30 - 40 MeV study of Fricke (Fr 67). The values obtained were in reasonable agreement with those obtained by Satchler at 30 MeV (Sa 67), by Greenlees and Pyle at 30 MeV (Gr 66) and by Fricke and Satchler at 40 MeV (Fr 65). The (p,d) study by Kashy (Ka 64) used parameters for 9 - 22 MeV scattering obtained by Perey (Pe 63a). One of the principal differences between the Perey and Fricke sets is that a much faster V(E) dependence is predicted in the earlier set. Table 4.1 lists the proton parameters used in this thesis.

Table 4.1 Proton optical model parameters.

V*	r_o	a	r_C	W	W_D
46.8 MeV	1.16 fm	0.75 fm	1.25 fm	3 MeV	4 MeV

r_{oI}	a_I	V_{so}	r_s	a_s
1.37 fm	0.63 fm	6.04 MeV	1.064 fm	0.738 fm

* V is given for ^{48}Ti at 35 MeV. In general:

$$V = 49.9 - 0.22E + 0.4Z/A^{1/3} + 26.4(N-Z)/A \text{ MeV}$$

Deuteron parameters used in previous (p,d) investigations (Ka 64, Sh 65) were taken from the 11 - 27 MeV study by Perey and Perey (Pe 63) which included no spin-orbit term. Most recent works include such a term, having the same geometry as the real well, and indicate that the real well depth should be approximately equal to the sum of typical proton and neutron depths (Pe 66). Thus, deuteron parameters for this thesis were estimated from (1) the 2.5 - 10 MeV set of Wilhjelm and Hansen (Wi 68), (2) the 11.8 and 21.4 MeV sets of Perey and Perey (Pe 66) and (3) the 34.4 MeV set of Newman, et al. (Ne 67).

Figure 4.1 shows the sample parameters and the choices made. The Wilhjelm set is plotted at 2.5 MeV where it gave the best fit. Extra weight was given here to the 20 - 35 MeV parameters, since most of the transitions studied produced deuterons of these energies. But since most energy dependence studies of optical parameter fits show no justification for varying anything but V, and since the more widely varying parameters seldom influenced the calculations strongly, all but V were taken to be independent of energy. The parameters used are also given in Table 4.2. Note that an imaginary volume term is not used.

Table 4.2 Deuteron optical model parameters.

V*	r_o	a	r_C	W_D
101 MeV	1.065 fm	0.81 fm	1.30 fm	10 MeV
r_{oI}	a_I	V_{so}	r_s	a_s
1.41 fm	0.75 fm	7 MeV	1.065 fm	0.81 fm

* V is given at 25 MeV. In general:

$$V = 117 - 0.627E_d \text{ MeV}$$

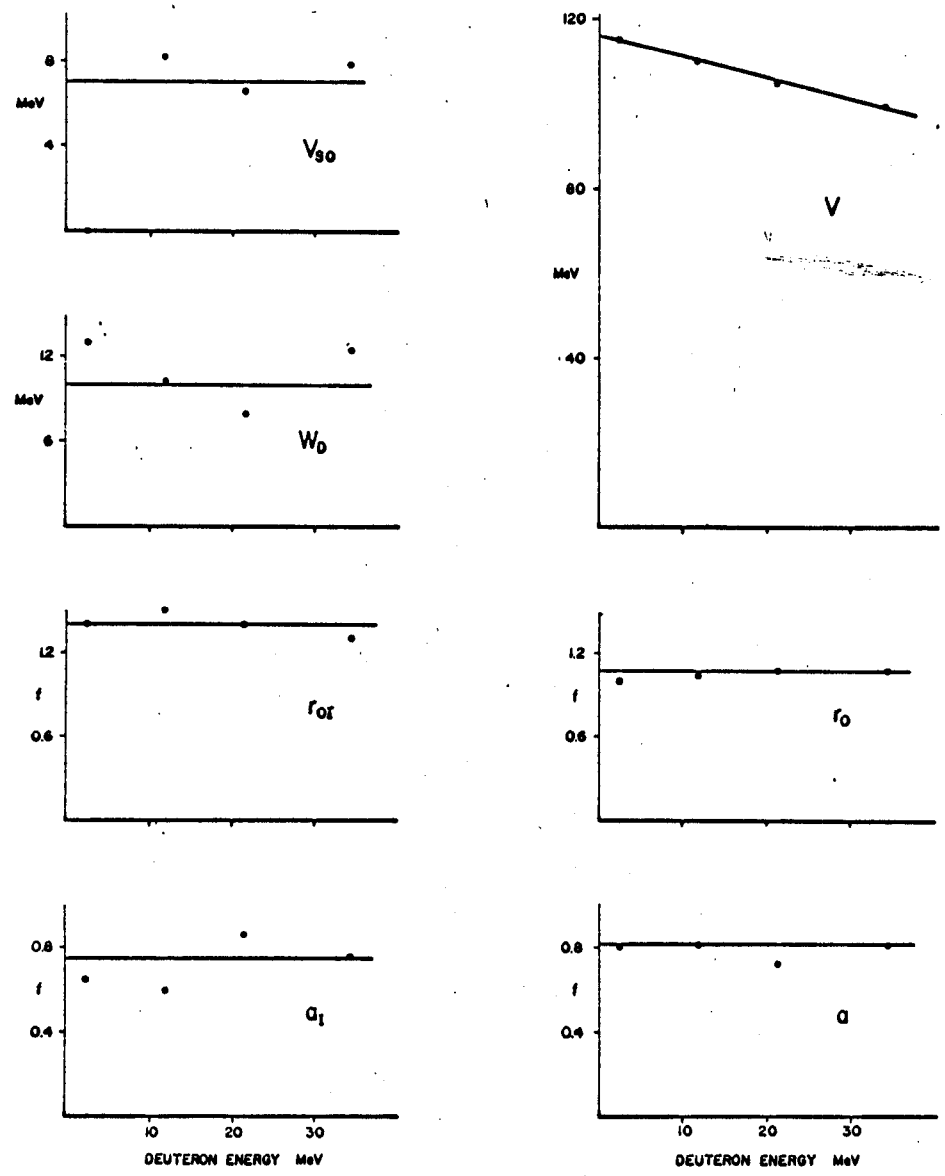

Figure 4.1 Deuteron optical model parameters.

To investigate the sensitivity of JULIE calculations to errors in the optical parameters, test cases were computed each with one of the parameters increased by ten per cent. Table 4.3 shows the results of this study for an L= 3 transfer at 25 MeV. The first three entries are for the neutron bound-state well, which employed the same (real) geometry used to describe elastic proton scattering. As expected, the dominant effects are caused by the real well depths and radii. The deuteron real parameters are surprisingly sensitive - a one per cent increase in radius causes a 4.7 per cent drop in peak cross-section (and a notable change in the shape of the cross-section). Care must be taken, therefore in interpreting absolute spectroscopic factors extracted.

Table 4.3 Per cent increase in peak (p,d) cross-section for ten per cent increase in parameter.

Parameter	Effect for p	Effect for d
r_o BSW	28 per cent	--
a^o BSW	8	--
r_C BSW	0	--
V^C	20	-47 per cent
r_o	20	-49
a^o	-2	5
r_C	0	-3
W^C	0	--
W_D	-2	-12
r_{oI}	-15	-21
a_I	-3	-17
V_{so}	0	0
r_s	0	--
a_s	0	--

5. ENERGY DEPENDENCE OF $^{48}Ti(p,d)^{47}Ti$

5.1 Experimental Results

Angular distributions of $^{48}Ti(p,d)^{47}Ti$ transitions have been measured over an angular range of eight to 90 degrees in the laboratory at 24.80, 29.82, 35.15, 39.97 and 45.05 MeV incident energies. Figure 5.1 shows a typical spectrum, aligned with the observed energy levels in ^{47}Ti. The L-transfer, J and T assignments for the strong transitions are taken from earlier studies (Ka 64, Sh 65, Ra 66, Ro 67).

Note that the principal transition occurs to the 0.16 MeV first excited state and not to the ground state. The latter is known to have spin 5/2-, and is expected to consist mostly of three $1f_{7/2}$ neutrons coupled to 5/2-. Since the direct pickup of a $1f_{7/2}$ neutron from a 0+ target cannot excite this state, the transition can only proceed in a direct process via $1f_{5/2}$ configuration admixtures in the target and final state wave functions. The 1f spin-orbit splitting is known to be on the order of 5.5 MeV in this mass region (Be 64) so the direct reaction cross-section for this channel is expected to be small (Be 65).

Thus the 0.16 MeV L= 3 transition is of prime importance in the energy dependence investigation. Also included in the study are the strong L= 1 transition at 1.54 MeV measured excitation and the L= 2 transfer at 1.81 MeV. The latter

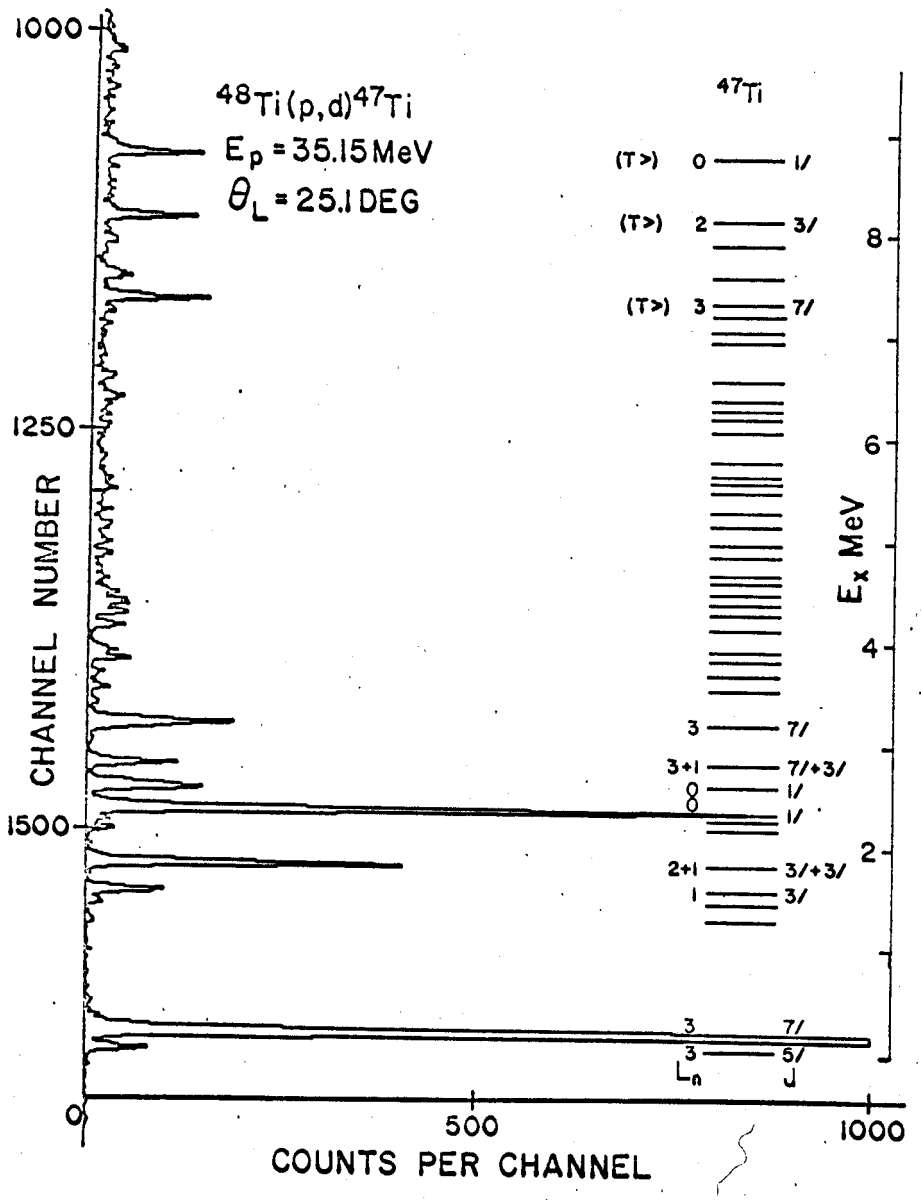

Figure 5.1 Deuteron spectrum from ^{48}Ti target and levels observed.

is known to be an unresolved doublet (Ra 66), which includes an L= 1 transition. This component is relatively weak, as will be shown later, and does not strongly influence the shape of the cross-section.

The three strong transitions between seven and nine MeV are to T= 5/2 analog states. One can locate such states by subtracting the n-p mass difference from the mass of the analogous state in ^{47}Sc, then adding the Coulomb energy required to bring an additional unit of charge into the nucleus. Systematics of Coulomb energies in this region have been investigated (Sh 67), and usually agree with observed analog excitations to within 100 keV. Analog state transitions stand out as concentrated deuteron groups against a nearly continuous background of states of lower T.

Above these analog states, in fact up to at least 20 MeV excitation, no significant transitions are observed. Thus one can characterize ^{48}Ti(p,d)^{47}Ti as leading principally to a few low-lying states in each isospin spectrum. Figures 5.2 and 5.3 show the odd-L and even-L transitions described above at the five incident energies. In addition, the strong L= 0 transfers measured at 2.35 and 8.74 MeV are displayed. Since these distributions are expected to have their principal maxima at zero degrees, they are not easily compared to calculated shapes and so play no role in the DWBA investigation.

All L= 3 cross-sections were found to increase quite

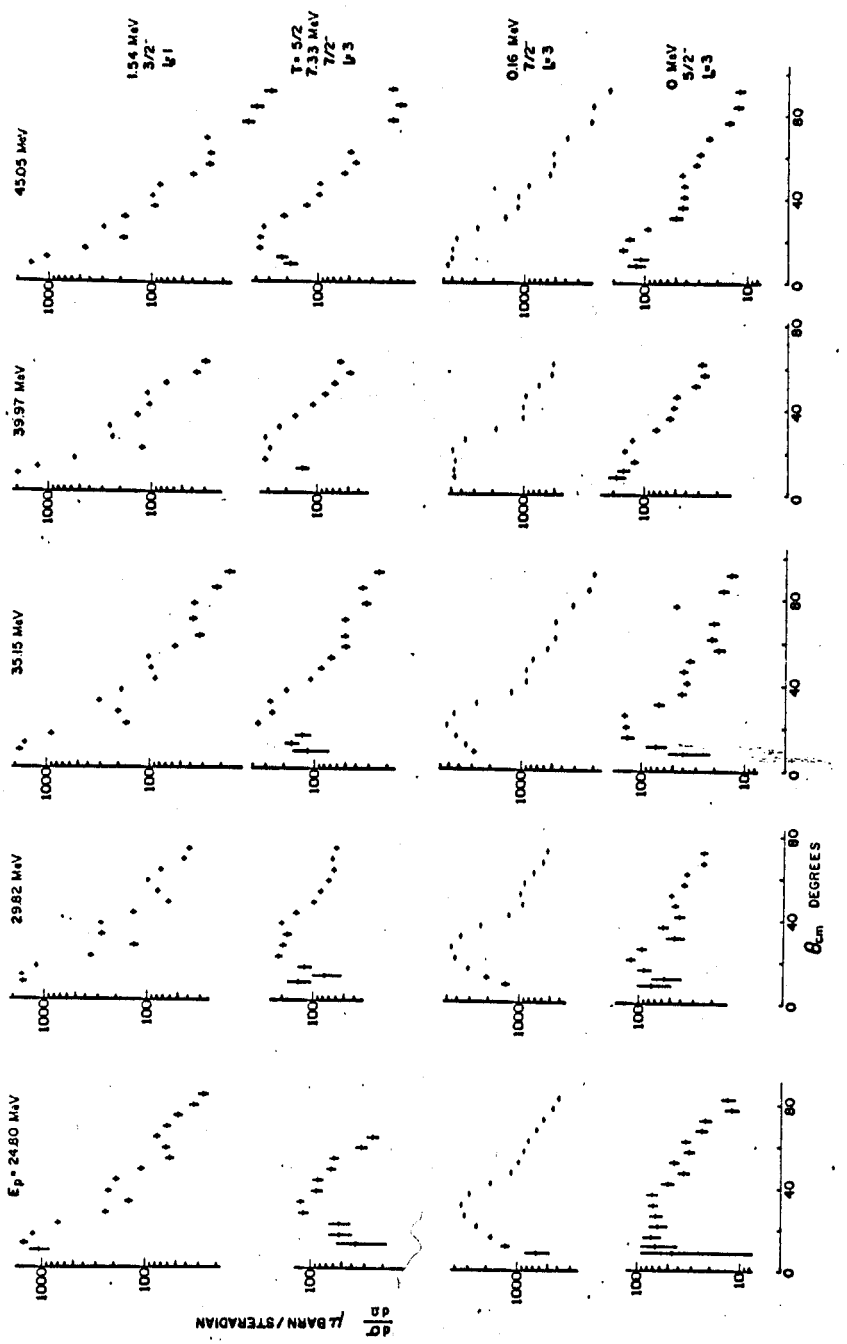

Figure 5.2 Energy dependence of odd-L transfers in $^{48}Ti(p,d)^{47}Ti$.

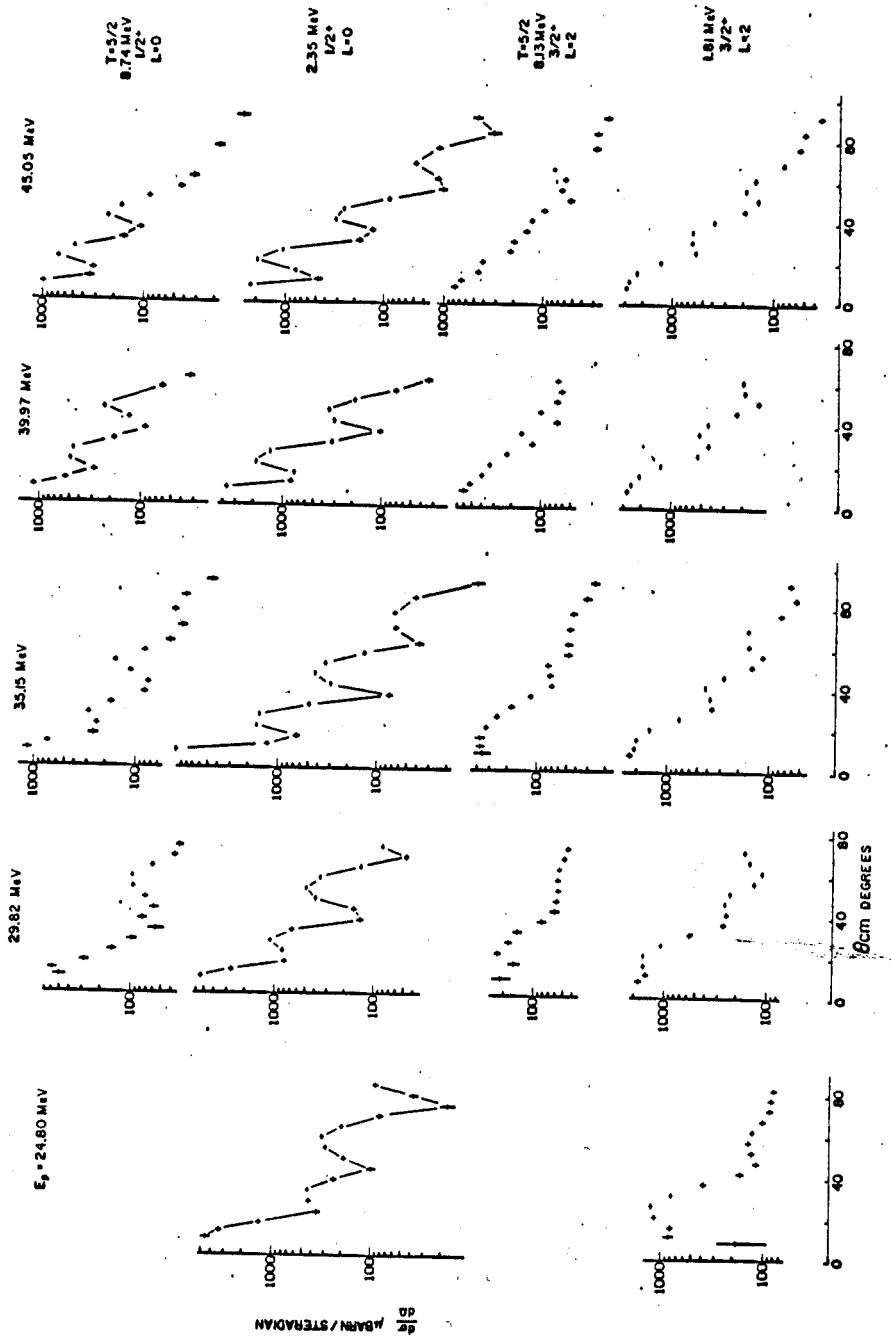

Figure 5.3 Energy dependence of even-L transfers in $^{48}Ti(p,d)^{47}Ti$.

linearly with energy up to about 35 MeV, then become fairly constant (see Figures 5.2 and 5.3). This is consistent with the data of Kashy and Conlon (Ka 64) and of Sherr, et al., at 28 MeV (Sh 65). The shape of these cross-sections, however, undergoes a marked change, the shape apparently being a function of the energy of the outgoing deuteron (compare 7.33 and 0.16 MeV L= 3 distributions). Other L-transfer cross-sections also increase with energy, but more uniformly. Such differences in energy dependence must, of course, be reproduced by the DWBA calculations to produce consistent spectroscopic factors.

5.2 Zero-Range DWBA Calculations

DWBA calculations were performed for the principal L-transfers described above at 25, 30, 35, 40 and 45 MeV. In all cases the neutron bound-state wave function was computed for a well having the same geometry as the proton elastic channel optical model. Neutron well depth was adjusted to bind the specified single-particle orbital with the correct spearation energy. The real well depths for the proton and deuteron elastic channels were selected for each case according to Tables 4.1 and 4.2.

In the zero-range approximation, the calculations included a series of lower integration cutoffs from zero to seven fm. to bracket the nuclear surface, which is at about $1.25A^{1/3}$ or 4.54 fm. Table 5.1 lists the spectroscopic factors

extracted for the principal L= 3 transition as a function of cutoff radius and energy. All cutoffs except at three fm exhibit a noticeable change with energy, usually a 30 per cent decline from 35 to 45 MeV. At each energy, S rises abruptly between two to four fm, passes through a local maximum near the surface and climbs steeply. The same study performed for the high-lying T= 5/2 L= 3 transition gave essentially identical results.

Table 5.1 Zero-range spectroscopic factors for the L= 3 transition to ^{47}Ti(0.16 MeV).

Cutoff	25 MeV	30 MeV	35 MeV	40 MeV	45 MeV
0 fm	3.0	2.7	2.7	2.3	1.9
2	3.0	2.7	2.7	2.4	1.9
3	3.1	3.2	3.4	3.4	3.0
4	5.6	5.3	5.4	4.8	3.6
5	5.0	4.8	4.8	4.0	3.3
6	6.6	5.4	6.4	5.6	4.9
7	11.8	12.9	14.1	13.7	11.7

Table 5.2 shows very similar results for L= 1, except that no energy dependence is observed out to three fm. Again a plateau occurs near the nuclear surface exhibiting energy dependence very similar to L= 3. Finally, a study of L= 2 spectroscopic factors showed (1) no energy dependence at zero cutoff, (2) a marked increase of S with energy at three fm, (3) a local minimum of S near the surface and (4) energy dependence for surface cutoffs nearly identical to that for L= 1 and L= 2.

The ability of DWBA to reproduce the shapes of experimental angular distributions is displayed in Figure 5.4. The

dashed curves are zero-range calculations with no integration cutoffs. In all cases, such calculations predict far too much scattering at back angles. Even fits to the principal maximum become so poor at higher energies that comparison with the data is moot. The solid lines represent zero-range calculations where the integration is cutoff near 4.5 fm. These curves track the data much more closely, particularly at back angles. While the agreement with data also deteriorates with increasing energy, it is better than for no cutoff.

Table 5.2 Zero-range spectroscopic factors for the L= 1 transition to ^{47}Ti(1.54 MeV).

Cutoff	25 MeV	30 MeV	35 MeV	40 MeV	45 MeV
0 fm	0.18	0.15	0.15	0.19	0.17
2	0.23	0.22	0.26	0.30	0.25
3	0.26	0.26	0.29	0.33	0.27
4	0.33	0.31	0.32	0.35	0.22
5	0.23	0.23	0.23	0.22	0.19
6	0.26	0.27	0.29	0.32	0.29
7	0.49	0.51	0.60	0.72	0.69

Thus, in the zero-range approximation, DWBA calculations with lower integration cutoffs at the nuclear surface appear to be the most reliable. They produce shapes which best approximate the data out of all cutoffs examined. They lead to spectroscopic factors which are quite constant for small changes in cutoff radius. Finally, they yield factors whose variation with energy, while not constant, is known for 25 - 45 MeV and is apparently independent of L-transfer or excitation energy. This conclusion agrees with the findings of Snelgrove (Sn 68) in the oxygen mass region.

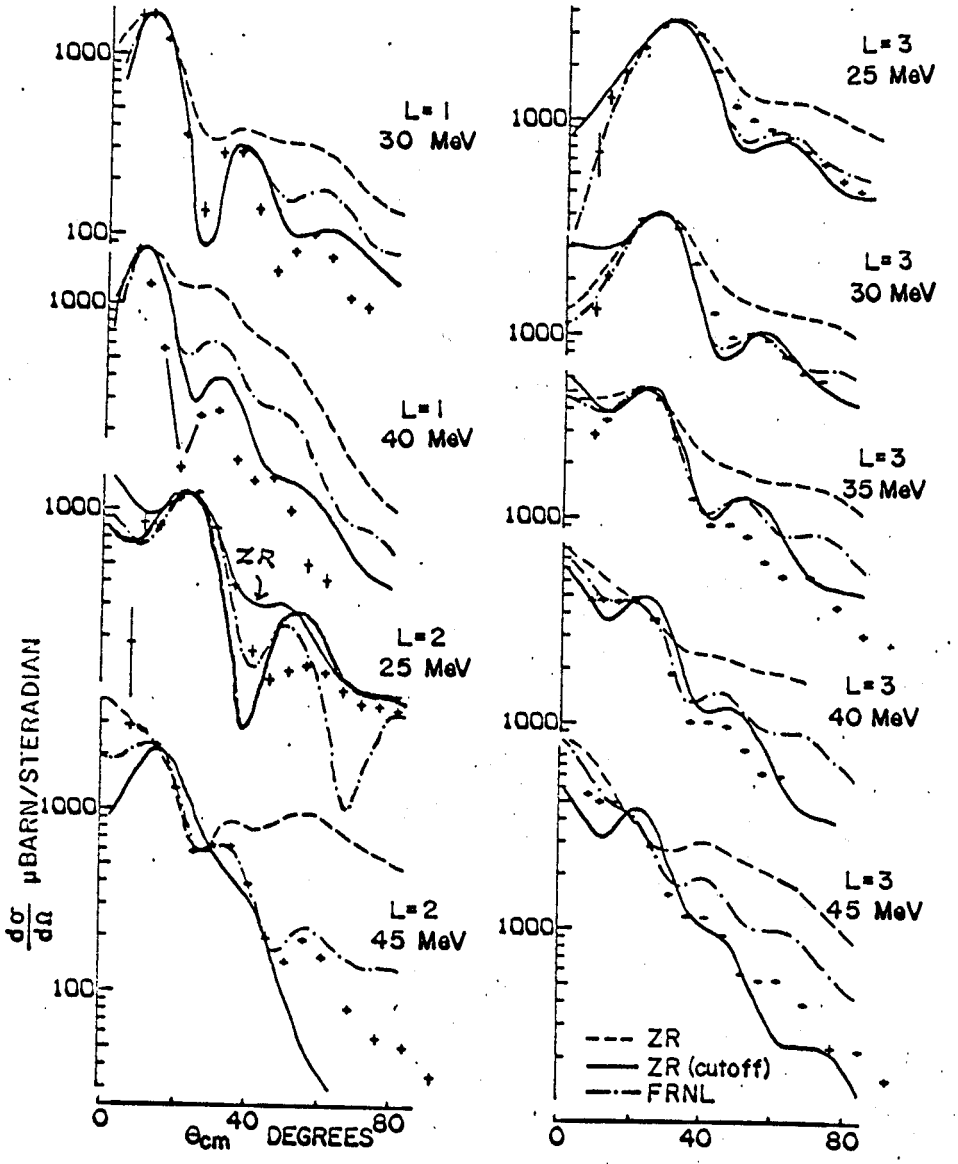

Figure 5.4 Some DWBA firs to $^{48}Ti(p,d)^{47}Ti$ for L= 1 (1.54 MeV), L= 2 (1.81 MeV) and L= 3 (0.16 MeV).

5.3 Finite Range DWBA Calculations

DWBA calculations were performed for the principal L-transfers described in Section 5.1 at 25, 30, 35, 40 and 45 MeV, using bound-state wave functions corrected for finite range and non-locality effects. Optical model parameters for the bound-state well and elastic channels were chosen as in the preceding section. The range of the interaction was taken as 1.5 fm, and the non-locality parameters were 0.85 fm for the proton and neutron and 0.54 fm for the deuteron.

The effect of integration cutoffs on FRNL spectroscopic factors has been investigated for the principal L= 3 transfer. There is no energy dependence for zero cutoff, and surface cutoffs behave much as those described above. The predicted shapes, however, are best for no cutoff and become much worse with increasing cutoff radius. Similar results were observed for the other L-transfers studied. Figure 5.4 shows the FRNL zero cutoff predictions as dot-dash lines. At 25 - 30 MeV they are generally better than zero-range with cutoff, but tend to be not as good at back angles for 40 - 45 MeV data.

It is concluded, then, that FRNL corrections produce results superior to the zero-range procedure described in the preceding section. The physical basis for FRNL is much better established than the computational artifice of discarding part of an integration. Predicted angular distributions

are of comparable quality. Finally, there is no apparent energy dependence from 25 to 45 MeV, as Table 5.3 shows for a variety of transitions. Note that the 0.16 MeV L= 3 measurements differ slightly from those in Table 5.3. This illustrates the limits of repeatabliity in the curve-matching process used to measure S. Fluctuations on the order of five per cent are, then, clearly not significant.

Predicted angular distributions, using FRNL corrections, deviate most from the data at back angles and at higher energies. Both are cases of large momentum transfer, or relatively deep penetration into the nucleus. From the study of integration cutoffs, it is evident that the deviations are caused by the nuclear interior contributing proportionately too much to the cross-section. Finite range and non-locality corrections damp this contribution (see Section 2.3), but apparently not enough.

Table 5.3 FRNL spectroscopic factors for some of the principal transitions to ^{47}Ti.

Ex	L	J	25	30	35	40	45
0 MeV	3	5/2	0.13	0.14	0.13	0.14	0.13
0.16	3	7/2	3.5	3.5	3.7	3.4	3.4
1.54	1	3/2	0.19	0.18	0.18	0.19	0.17
1.81	2	3/2	2.1	2.2	1.9	1.8	1.9
7.33	3	7/2	0.46	0.54	0.52	0.47	0.45

Green (Gr 67) has investigated yet another possible correction, for the dependence of the p-n interaction on the density of nuclear matter. As in the case of finite range and non-locality, this correction tends to damp

contributions from the nuclear interior. At present calculations have been performed only for the oxygen mass region. There the agreement of DWBA with (p,d) data is markedly improved by using this correction (Sn 69). The results of this thesis indicate that performing density-dependent corrections for titanium would result in similar improvement.

SPECTROSCOPY OF (p,d) REACTIONS

6.1 $^{48}Ti(p,d)^{47}Ti$

The general features of $^{48}Ti(p,d)^{47}Ti$ were discussed in Section 5.1, and are displayed in Figure 5.1. Based on the conclusions of Chapter 5, it was decided to study the spectroscopy of this reaction at 35.15 MeV, using FRNL corrections with no integration cutoffs in all DWBA calculations. Table 6.1 summarizes the observed data and spectroscopic analysis. The measured cross-sections for all observed transitions are displayed in Figures 6.1, 6.2 and 6.3.

Measured excitation energies are given in the first column of Table 6.1, followed by energies recalibrated to agree with the magnetic spectrograph study, by Rosner and Pullen (Ro 67), of the analog state spectra of $^{45,47,49}Ti$. Low-lying states are compared with the precision $^{46}Ti(d,p)^{47}Ti$ study by Rapaport, Sperduto and Buechner (Ra 66) and the (d,p) J-dependence study by Lee and Schiffer (Le 67). Earlier (p,d) investigations of ^{47}Ti levels have been made by Kashy and Conlon (Ka 64) and by Sherr, et al. (Sh 65). Finally, there are the more recent (^{3}He,^{4}He) studies by L'Ecuyer and St.-Pierre and by Lutz and Bohn (L'E 67, Lu 68). All previously established levels are included in the table down to the dashed line. Below this line the level density is too high for meaningful comparisons.

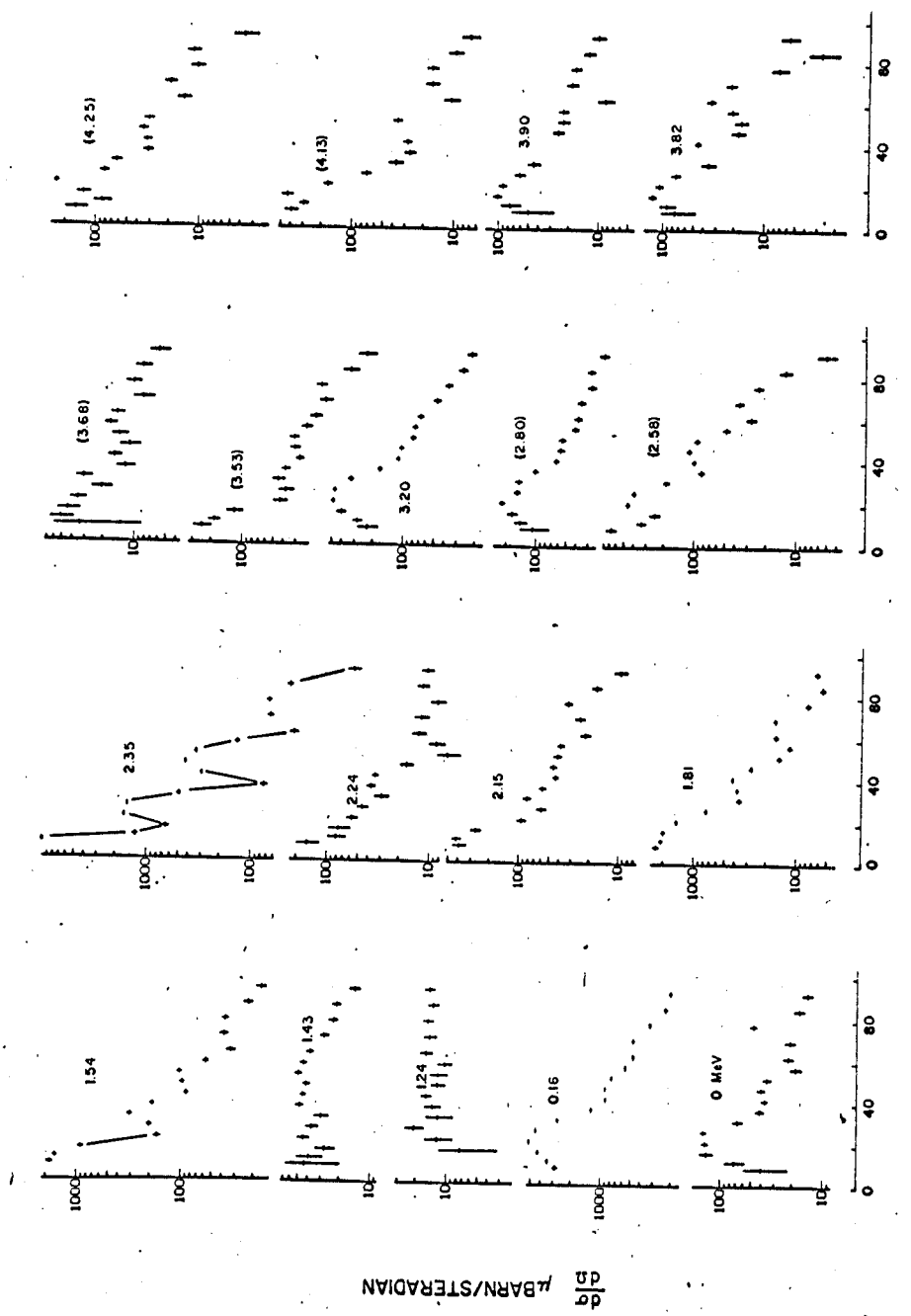

Figure 6.1 Measured angular distributions of $^{48}Ti(p,d)^{47}Ti$ at 35.15 MeV, Ex= 0 - 4.24 MeV.

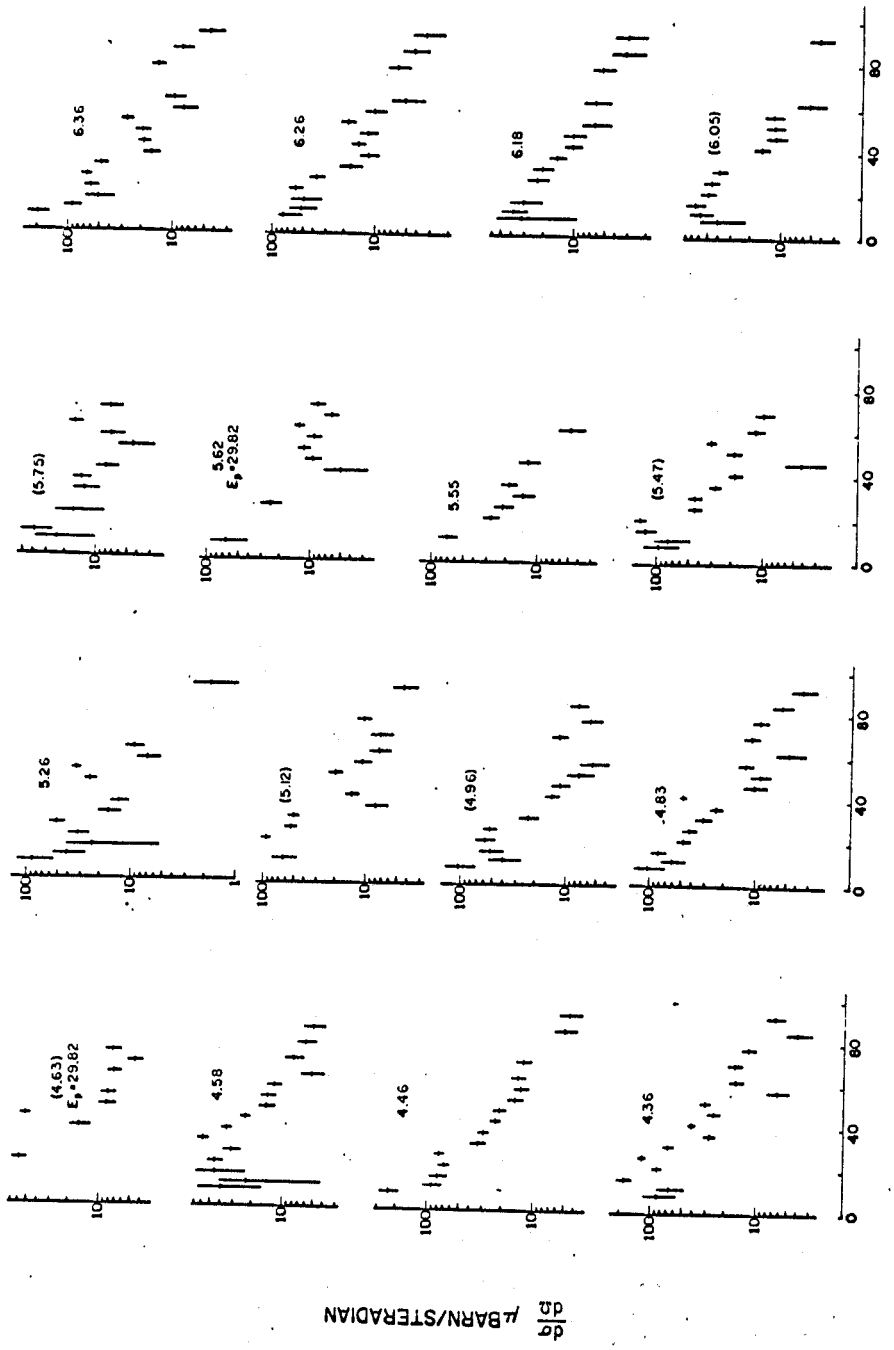

Figure 6.2 Measured angular distributions of $^{48}Ti(p,d)^{47}Ti$ at 35.15 MeV, Ex= 4.36 - 6.36 MeV.

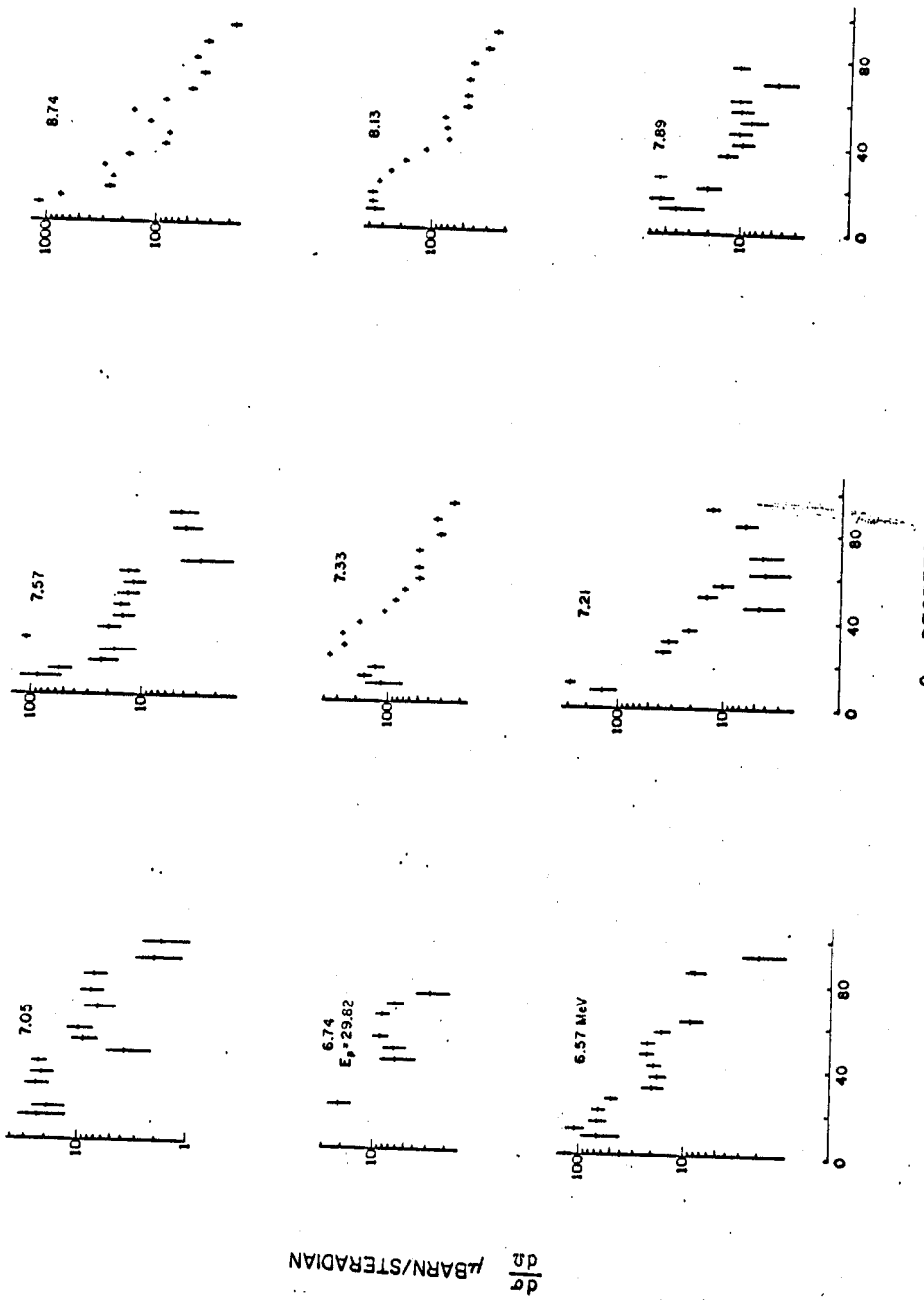

Figure 6.3 Measured angular distributions of $^{48}Ti(p,d)^{47}Ti$ at 35.15 MeV, Ex= 6.57 - 8.74 MeV.

Table 6.1 Summary of results for $^{48}Ti(p,d)^{47}Ti$ at 35.15 MeV.

MEASURED				ASSIGNED				PREVIOUS	
Ex a MeV	Ex b MeV	σmax mb/sr	θmax deg.	L	J	S	T	Ex MeV	J
0	0	0.14	22	3	5/2-	0.12	3/2	0	5/2-
0.16	0.16	5.1	20	3	7/2-	3.6		0.157	7/2-
1.24	1.25	0.02	flat					1.247	
1.43	1.44	0.05	30-60	(5)	(9/2-)	0.01		1.442	
1.54	1.55	1.8	8	1	3/2-	0.15		1.545	3/2-
1.81	1.82	0.48	8	1	(3,1/2)	0.04		1.788	1/2-
		1.8	16	2	3/2+	1.9		1.816	3/2+
2.15	2.16	0.40	10	1	(3/2-)	0.03		2.157	(1,3/2)
2.24	2.26	0.16	@8					2.252	
								2.292	
2.35	2.37	1.6	22c	0	1/2+	(0.59)		2.361	1/2+
2.58	2.60	0.22	22c	0	1/2+	(0.08)			1/2+
		0.25	20	3	7/2-	0.29			
2.80	2.82	0.22	22	3	7/2-	0.25			(L= 3)
3.20	3.22	0.48	22	3	7/2-	0.46			7/2-
3.53	3.55	0.24	6	1	(3/2-)	0.03		3.545	3/2-
3.68	3.70	0.05	12						
3.82	3.84	0.12	18						
3.90	3.92	0.10	18						
4.13	4.15	0.14	8	(1)		0.02			
		0.14	16	(2)		0.37			
4.25	4.28	0.24	@20						
4.36	4.38	0.18	@16						
4.46	4.48	0.23	@8						
4.58	4.62	0.06	@30						
4.63	4.67								
4.83	4.86	0.10	@8						
4.96	4.99	0.10	@8						
5.12	5.16	0.09	@20						
5.26	5.30	0.09	@8						

Table 6.1 continued

MEASURED				ASSIGNED				PREVIOUS	
Ex a MeV	Ex b MeV	σmax mb/sr	θmax deg.	L	J	S	T	Ex MeV	J
5.47	5.51	0.14	@20						
5.55	5.59	0.01	@20						
5.62	5.66								
5.75	5.79	0.04	@12						
6.05	6.09	0.06	@16						
6.18	6.23	0.04	@12						
6.26	6.31	0.08	@8						
6.36	6.40	0.19	@8						
6.57	6.61	0.11	@12						
6.74	6.78								
7.05	7.10	0.02	10-40						
7.21	7.25	0.14	@8						
7.33	7.38	0.26	28	3	7/2-	0.46	5/2	7.38	7/2-
7.57	7.62	0.09	@8						
7.89	7.94	0.06	16						
8.13	8.18	0.37	14	2	3/2+	1.4	5/2	8.18	3/2+
8.74	8.80	0.29	22c	0	1/2+	(0.80)	5/2	8.80	1/2+

Notes: a) Excitations measured b) Corrected excitations
c) Second maximum

Since DWBA predictions are usually compared to data at the principal maximum, the cross-section in millibarns per steradian and the center-of-mass angle in degrees is listed at this point. If the distribution has no definite peak, the largest value measured is given, followed by the angle at which it was measured flagged with an @ sign. An exception is any state assigned L= 0, for which the data on the second maximum is recorded.

Several angular distributions measured were known or suspected to arise from unresolved doublets of different L-values. In such a case, least-squares fits were performed of the six possible linear combinations of two pure L= 0 - 3 distributions. From the variances of the fits, the most likely combination was determined. The computed variances of the coefficients, obtained from the inverted least-squares matrix (Mo 60), indicated the validity of the fit and the sensitivity to individual contributions. Where such a fit has been made to the data, two lines of cross-section are given, indicating the maximum for each contribution.

L-transfers are generally determined by comparison with known transitions, aided in some cases by DWBA predictions. Strong non-zero L-transfers are almost always assigned to the $1d_{3/2}$, $1f_{7/2}$, or $2p_{3/2}$ shells because these lie nearest the Fermi surface. Following the usual convention, parentheses indicate tentative assignments. Thus, all L= 0 assignments are given only tentative spectroscopic factors, due to the

difficulty of comparing data to DWBA calculations. Isospin assignments are always to the lower allowed T unless specifically stated otherwise.

As Table 6.1 reveals, the qualitative description of this reaction given in Section 5.1 is quite precise - there are two isospin spectra, each with only a few strong transitions. A comparison with the predicted L= 3 transfers in Table 2.1 shows qualitative similarities between the data and the MBZ spectrum, but not enough to warrant close scrutiny. The levels of interest are the two unusual assignments at 1.44 and 1.81 MeV. The former is a very weak transition having a definite direct reaction character, but peaking far back in angle. DWBA calculations for L= 5 reproduce the wide change in peak angle observed from 25 to 45 MeV. If the L assignment is correct, $1h_{9/2}$ is the lowest-lying candidate, closely corresponding to a 9/2- state predicted by MBZ (Mc 64a). The L= 1 component of the doublet at 1.81 MeV has been assigned spin 1/2- on the basis of J-dependence in back angle scattering (Le 67). If this much $2p_{1/2}$ admixture is known to occur, then weak L= 1 assignments cannot be assigned a definite J in this study.

The large body of states between four and seven MeV are too small to permit reliable assignment of L values. Many show a direct reaction distribution, however, having a strong dependence on scattering angle. Of these, it can only be concluded that they represent fairly complex configurations in terms of single particle states, and that they may account

for a significant fraction of the total reaction strength. It should be emphasized that the excitation energies and distributions reported for this region are not necessarily for discrete states; rather they represent peaks in the (p,d) cross-section.

6.2 ^{46,50}Ti(p,d)^{45,49}Ti

The ^{50}Ti(p,d)^{49}Ti reaction was measured at 45.05 MeV over an angular range of eight to 60 degrees in the laboratory. Figure 6.4 shows a typical deuteron spectrum obtained from the ^{50}Ti foil, along with the levels observed. Since the target was 23 per cent ^{47}Ti (see Table 3.1), its strong transitions are also indicated. L, J and T assignments for the principal transitions are taken from earlier work (Ka 64, Sh 65, Ba 67, An 69).

Besides the titanium studies mentioned in the previous section (Ka 64, Sh 65, L'E 67, Ro 67, Lu 68), other investigations of the levels of ^{49}Ti include the precision (d,p) work of Barnes, et al., at 6.2 MeV (Ba 67) and the consistent level scheme developed by Anderson, et al. (An 69). The measured angular distributions are presented in Figures 6.5 and 6.6, and results of the spectroscopic study are summarized in Table 6.2. The same general remarks apply to this table as were made in the preceding section concerning Table 6.1. All known levels (An 69) are presented, down to the dashed line, below which only states corresponding to observed

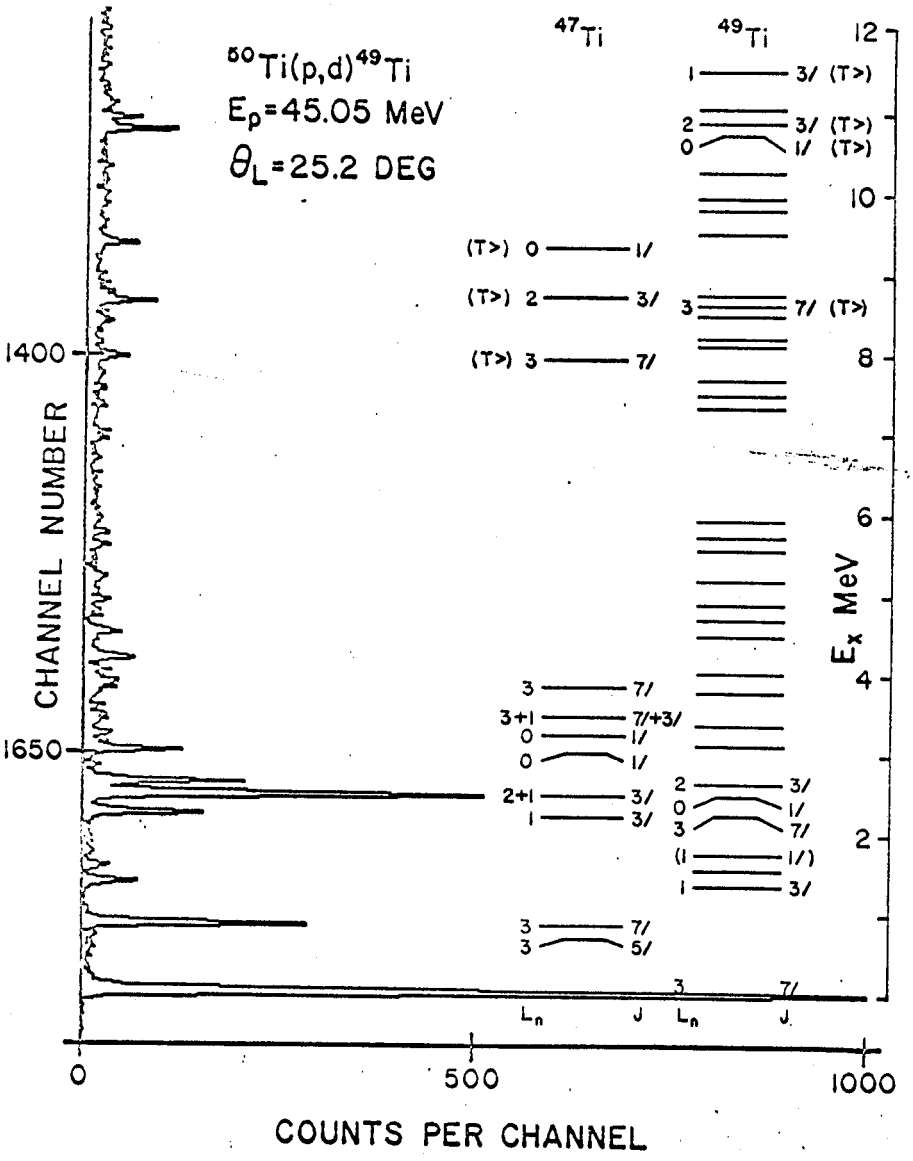

Figure 6.4 Deuteron spectrum from ^{50}Ti target and levels observed.

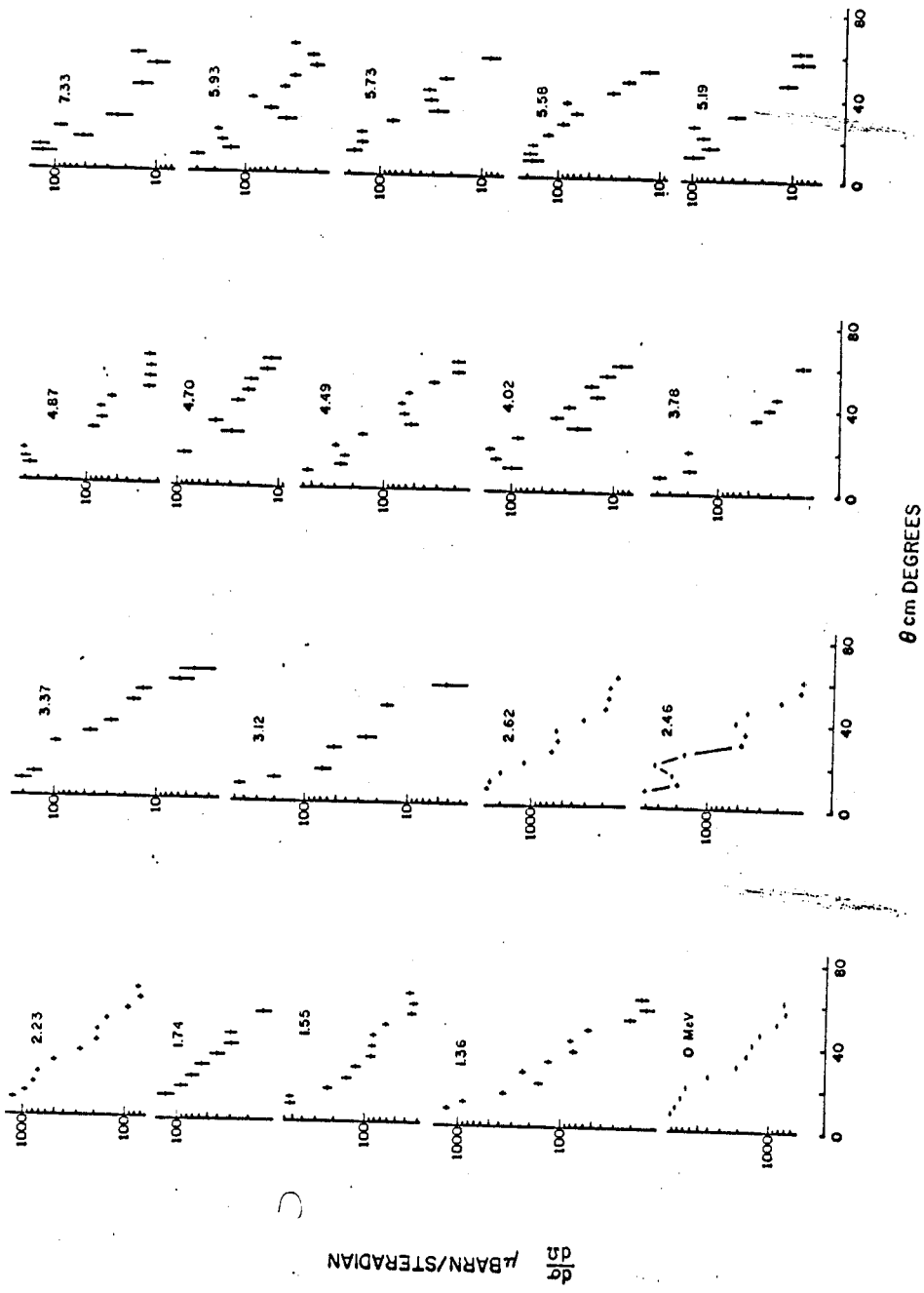

Figure 6.5 Measured angular distributions of $^{50}Ti(p,d)^{49}Ti$ at 45.05 MeV, Ex= 0 - 7.33 MeV.

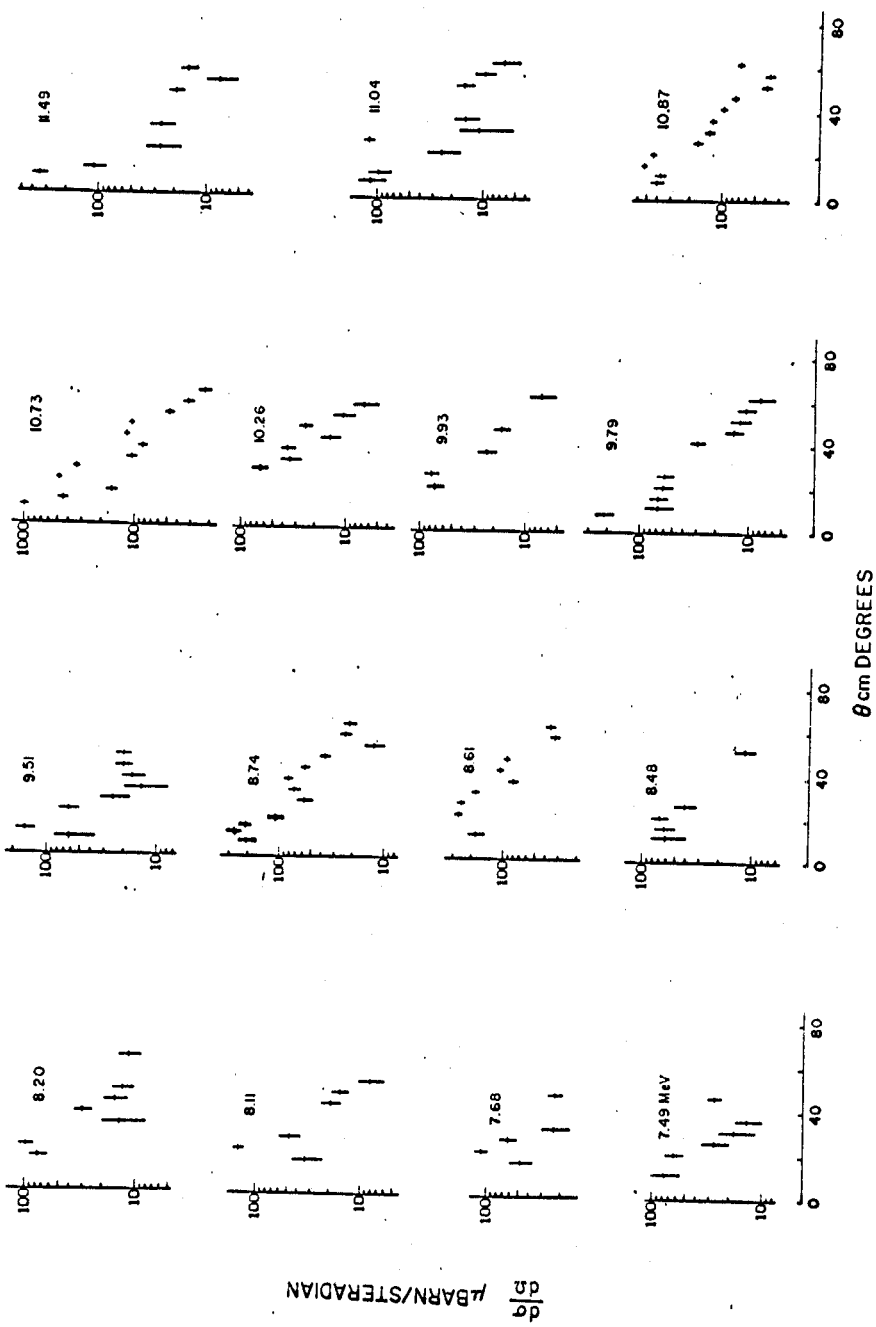

Figure 6.6 Measured angular distributions of $^{50}Ti(p,d)^{49}Ti$ at 45.05 MeV, Ex= 7.49 - 11.49 MeV.

Table 6.2 Summary of results for $^{50}Ti(p,d)^{49}Ti$ at 45.05 MeV.

MEASURED				ASSIGNED				PREVIOUS	
Ex a MeV	Ex b MeV	σmax mb/sr	θmax deg.	L	J	S	T	Ex MeV	J
0	0	9.0	8	3	7/2-	3.6	5/2	0	7/2-
1.36	1.38	1.3	8	1	3/2-	0.19		1.382	3/2-
								1.542	
1.55	1.58	0.48	8	1	3/2-	0.07		1.586	(3/2-)
		0.04						1.622	
								1.724	1/2-
1.74	1.77	0.12	8	(3)		(0.05)		1.762	
2.23	2.27	1.2	8	3	7/2-	0.58		2.261	(7/2-)
								2.472	
2.46	2.50	2.5	20c	0	1/2+	(1.5)		2.503	1/2+
								2.505	
		1.3	8	(3,2)		(0.6,1.2)		2.516	7,5/2-
								2.557	
2.62	2.66	2.6	10	2	3/2+	2.4		2.665	3/2+
3.12	3.17	0.44	8	1	(1,3/2)	0.08		3.176	1/2-
3.37	3.42	0.20	8	1	(1,3/2)	0.04		3.430	(1,3/2)
3.78	3.84	0.17	8	(3)	(7/2-)	0.10		3.847	(7,5/2)
		0.05	20c	(0)	(1/2+)	(0.03)			
4.02	4.08	0.16	18						
4.49	4.56	0.29	18						
4.70	4.78	0.08	@15						
4.89	4.97	0.40	12						
5.19	5.28	0.10	@12						
5.58	5.67	0.18	8						
5.73	5.82	0.18	@12						
5.93	6.03	0.27	8						
7.33	7.45	0.14	@12						
7.49	7.61	0.08	@12						
7.68	7.81	0.11	20						
8.11	8.24	0.14	@20						
8.20	8.33	0.10	@20						
8.48	8.62	0.07	20						
8.61	8.75	0.26	22	3	7/2-	0.23	7/2	8.75	7/2-
8.74	8.89	0.26	12	2	(5/2+)	0.48			
9.51	9.66	0.15	12						
9.79	9.95	0.21	8						
9.93	10.1	0.08	@26						
10.3	10.4	0.07	@26						
10.7	10.9	0.47	22c	0	1/2+	(0.77)	7/2	10.99	3/2+
10.9	11.1	0.51	16	2	3/2+	1.7	7/2	11.12	1/2+
11.0	11.2	0.12	@8						
11.5	11.7	0.34	@8	(1)		1.0	(7/2)		

Notes: a) Excitations measured b) Corrected excitations
c) Second maximum

(p,d) transitions are reported (An 69, Ro 67).

Comparing this data to $^{48}Ti(p,d)^{47}Ti$, one is again struck by the selectivity of the (p,d) reaction. There is the strong L= 3 transition, this time to the ground state, a few strong low-lying transitions, a wide gap and then the analog states. Again the similarity to the MBZ predictions of table 2.1 is only qualitative.

Of the states previously assigned spin 1/2-, the one at 1.724 MeV is not seen and that at 3.176 apparently only weakly. For the doublet at 2.46 MeV measured excitation, it was not possible to distinguish between an L= 0 + 2 and an L= 0 + 3 assignment. Due to the similarity of L= 2 and L= 3 angular distributions at this energy, several assignments are uncertain.

A strong L= 2 transition was observed at 8.74 MeV which is not a candidate for being an analog state. It is believed that this may be a $1d_{5/2}$ hole state, since it lies at about the excitation predicted by the simple shell model (Figure 2.1). Such a state would be much less likely to be spread in this nucleus, since promoting a neutron from the core closes the outer neutron shell and severely restricts the possible couplings. Finally, a fairly strong transition was measured at 11.5 MeV which has been tentatively assigned L= 1 and may be an analog state.

The $^{46}Ti(p,d)^{45}Ti$ reaction was measured over an angular range of eight to 70 degrees in the laboratory at an incident

energy of 34.75 MeV. Figure 6.7 shows a typical spectrum, with the observed levels and principal contaminants. L, J and T are given for the strongest transitions.

Since ^{44}Ti is not stable, (d,p) stripping information is not available. The principal transitions have been reported (Ka 64, L'E 67), and the excitations established for the analog states (Ro 67). A low-lying triplet (0 (7/2-), 37 (3/2-), 40 keV) has been reported by Jett, Jones and Ristinen (Je 68), for which some evidence has been found in this thesis, but other levels reported at 0.744 and 1.227 MeV are not observed. A level scheme based on 26 MeV (p,d) data has also been reported by Jones, Johnson and Jett (Jo 68), which gives excitation energies as much as seven per cent different than those reported here. The assigned L-transfers for the first few states agree, however.

Measured angular distributions are presented in Figures 6.8 and 6.9, and the findings are summarized in Table 6.3. The reaction strength is more uniformly distributed than for the other isotopes studied, but bears the same qualitative features. Only ten states have cross-sections greater than 0.15 mb/sr, four of which are assigned T= 3/2. Thus the (p,d) reaction is highly selective for all three targets.

The lowest-lying transition has been fit with L= 3 + 1 distributions, which is consistent with a low=lying (7/2, 3/2, 5/2) triplet (Je 68). Likewise the lowest analog transition, clearly a doublet in Figure 6.7, is best fit with L= 3 + 2, as expected (Ro 67). An L= 1 transition observed at

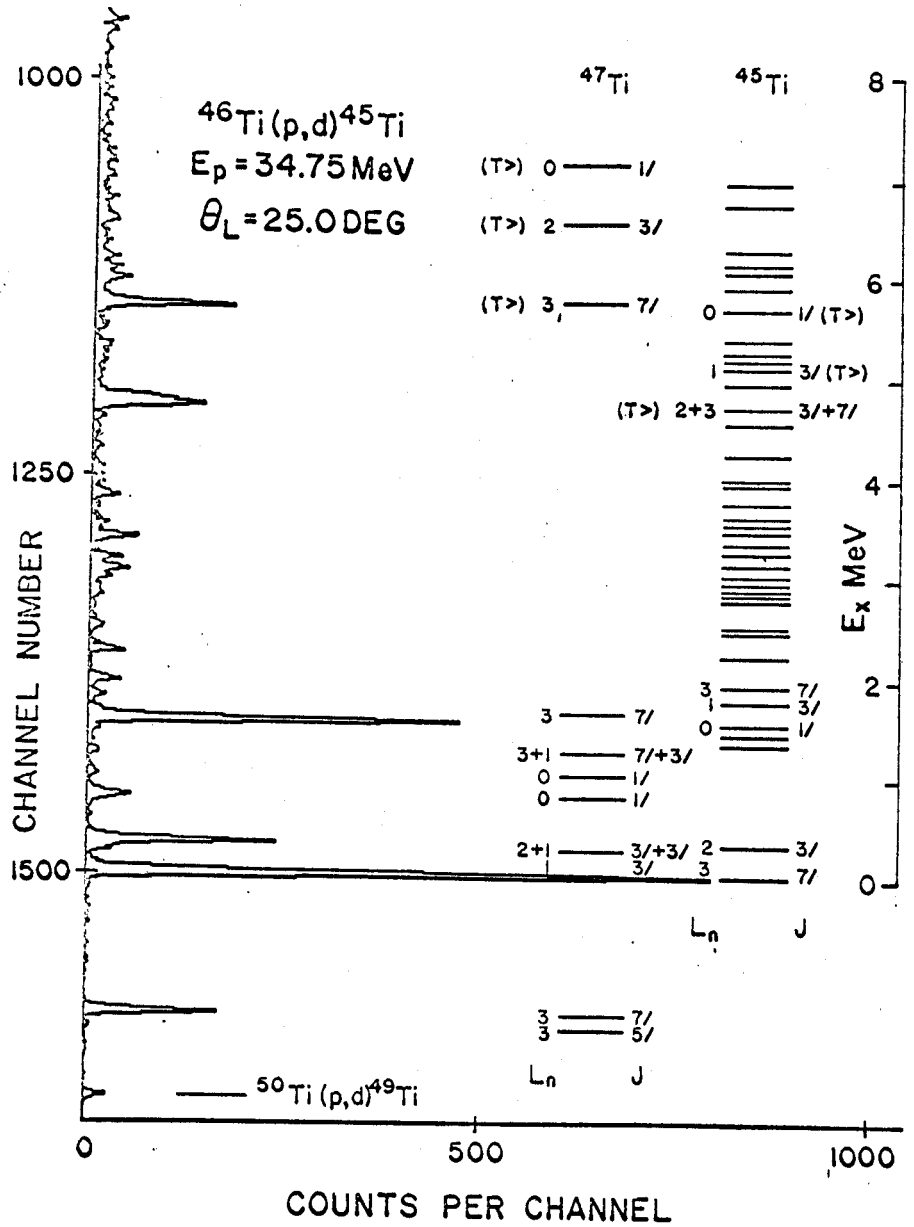

Figure 6.7 Deuteron spectrum from ^{46}Ti target and levels observed.

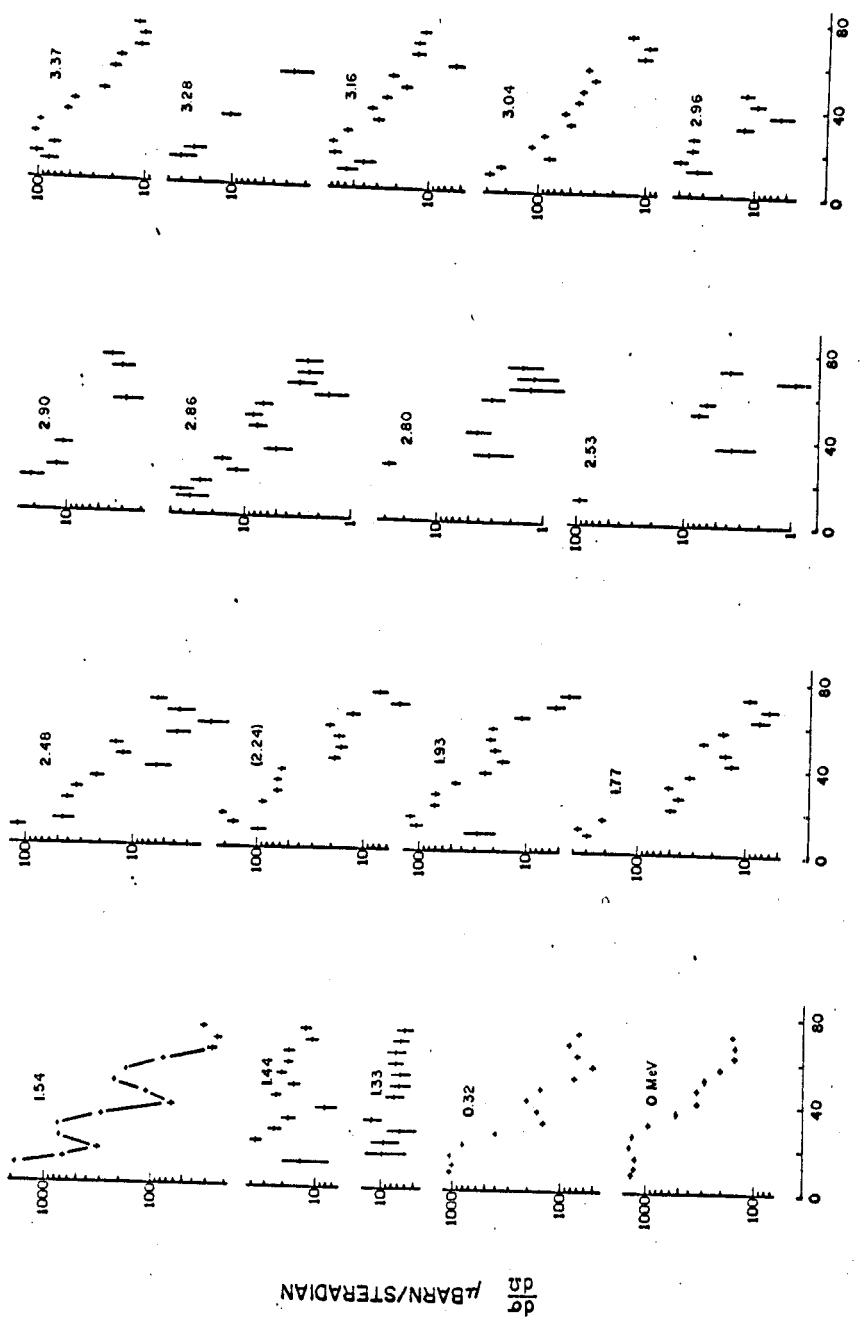

Figure 6.8 Measured angular distributions of $^{46}Ti(p,d)^{45}Ti$ at 34.78 MeV, Ex= 0 - 3.37 MeV.

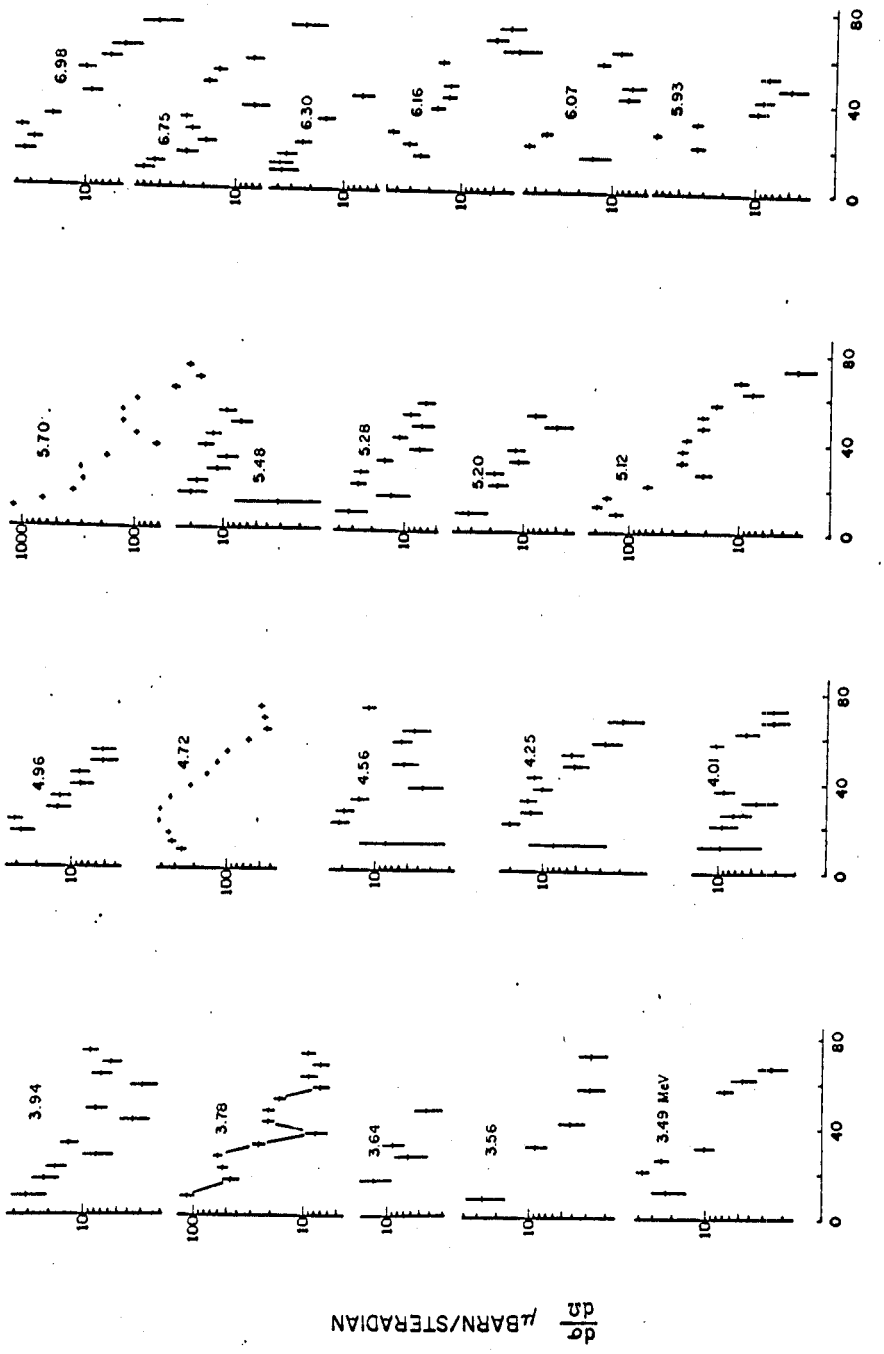

Figure 6.9 Measured angular distributions of $^{46}Ti(p,d)^{45}Ti$ at 34.78 MeV, Ex= 3.49 - 6.98 MeV.

Table 6.3 Summary of results for $^{46}Ti(p,d)^{45}Ti$ at 34.78 MeV.

MEASURED				ASSIGNED				PREVIOUS	
Ex a MeV	Ex b MeV	σmax mb/sr	θmax deg.	L	J	S	T	Ex MeV	J
0	0	1.4	22	3	7/2-	1.2	1/2	0	7/2-
		0.30	12	1	3/2-	0.33		0.037	(3/2-)
0.32	0.32	1.0	14	2	3/2+	1.0			3/2+
1.33	1.35	0.01	flat						
1.54	1.56	0.74	25c	0	1/2+	(0.33)			1/2+
1.77	1.79	0.35	12	1	(3/2-)	0.05			3/2-
1.93	1.95	0.07	22	3	(7/2-)	0.07			7/2-
2.24	2.26	0.07	22	(3)					3/2+
		0.15	12	(1)					
2.48	2.50	0.04	22c	(0)	(1/2+)	(0.02)			
2.53	2.55	0.09	@8						
2.80	2.82	0.03	@26						
2.86	2.88	0.04	10						
2.90	2.93	0.02	@16						
2.96	2.98	0.05	18						
3.04	3.07	0.08	22c	(0)	(1/2+)	(0.05)			
		0.09	14	(2)	(3/2+)	0.15			
3.16	3.19	0.08	18						
3.28	3.31	0.03	@12						
3.37	3.40	0.11	20	3	(7/2-)	0.14			
3.49	3.52	0.04	20						
3.56	3.59	0.03	@8						
3.64	3.67	0.01	@16						
3.78	3.82	0.06	22c	0	1/2+	(0.04)			
3.94	3.98	0.03	@8						
4.01	4.05	0.01	flat						
4.25	4.29	0.02	@20						
4.56	4.60	0.02	@20						
4.72	4.76	0.42	22	3	7/2-	0.62	3/2	4.74	7/2-
		0.18	14	2	3/2+	0.50	3/2	4.81	3/2+
4.96	5.00	0.03	20						
5.12	5.16	0.19	12	1	3/2-	0.04	(3/2)		
5.20	5.25	0.03	@8						
5.28	5.33	0.03	@8						
5.48	5.53	0.02	@16						
5.70	5.75	0.30	22c	0	1/2+	(0.40)	3/2	5.75	1/2+
5.93	5.98	0.03	@20						
6.07	6.12	0.06	@20						
6.16	6.21	0.04	28						
6.30	6.36	0.04	12						
6.75	6.81	0.07	8						
6.98	7.04	0.04	20						

Notes: a) Excitations measured b) Corrected excitations
c) Second maximum

5.12 MeV is a good candidate for a 3/2- analog state. No transitions of any significant strength were observed above six MeV.

6.3 Sum Rules and Q Dependence

Having made a spectroscopic analysis of the (p,d) data obtained, one is now in a position to test the sum rules put forth in Section 2.2 (or, contrariwise, to use the sum rules to test the spectroscopic factors extracted). Table 6.4 lists the summed spectroscopic factors for the $2s_{1/2}$, $1d_{3/2}$, $1f_{7/2}$ and outer shells for each of the three reactions studied. The sums are further divided into lower- and upper-T transitions, and ratios of experimental results to the predictions of Table 2.2 are obtained. Although it is of questionable validity, the analysis is carried through for L= 0.

It should be emphasized from the start of this discussion that the absolute normalization of these sums is open to some question. The results given in Chapter 4 show that the peak DWBA cross-section is quite sensitive to small changes in the optical model parameters used to describe the incident and exit channels and the bound-state wave function. Systematic errors on the order of 20 to 30 per cent are not unexpected. Moreover, an unknown amount of strength can go into many small levels, and so be lost to the sums.

Even granting these limitations, many of the results in

Table 6.4 Comparison of summed spectroscopic factors to predictions.

Tgt.	Shell	TOTAL		LOWER-T			UPPER-T		
		Exp.	Th.	Exp.	Th.	Ex/Th	Exp.	Th.	Ex/Th
^{46}Ti	$2s_{1/2}$	0.84	2	0.44	1.33	0.33	0.40	0.67	0.60
	$1d_{3/2}$	1.7	4	1.2	2.67	0.43	0.50	1.33	0.38
	$1f_{7/2}$	2.0	4	1.41	3.33	0.42	0.62	0.67	0.93
	outer	0.4	0	0.38			0.04		
^{48}Ti	$2s_{1/2}$	1.5	2	0.67	1.60	0.42	0.80	0.40	2.0
	$1d_{3/2}$	3.7	4	2.3	3.20	0.72	1.4	0.80	1.8
	$1f_{7/2}$	5.1	6	4.6	5.60	0.82	0.46	0.40	1.2
	outer	0.4	0	0.40			0		
^{50}Ti	$2s_{1/2}$	2.2	2	1.5	1.71	0.88	0.77	0.29	2.7
	$1d_{3/2}$	4.1	4	2.4	3.43	0.70	1.7	0.57	3.0
	$1f_{7/2}$	5.2	8	5.0	7.71	0.65	0.23	0.29	0.79
	outer	1.4	0	0.38			1.0		

Table 6.4 are absurd. If the sums are to be believed, fully half the expected number of particles are missing from the s-d shell in ^{46}Ti, while essentially all are accounted for in the heavier two nuclei. The likely explanation here is that much more of the (p,d) strength is unaccounted for, proportionately, since the cross-sections are observed to be more uniform and since no (d,p) spectroscopy is available to help identify weaker transitions. Doubling all sums for ^{46}Ti would also bring the $1f_{7/2}$ sum more into line.

One can argue that the 0.9 $1f_{7/2}$ neutrons missing from ^{48}Ti is within reason, but it is difficult to explain away nearly three from ^{50}Ti, particularly since it is expected to be a closed-shell nucleus. Again the sums insist this is not so, indicating that 1.4 of the missing neutrons are in the 2p shell. Yet the lighter nuclei promote only 0.4 neutrons to this shell. Clearly something is wrong.

The sums of transitions to upper-T states are uniformly larger than expected. An extreme case is the high-lying L= 1 transfer to ^{49}Ti which has S= 1 even though the lower-T sum is only 0.38. The common feature of these analog states that could lead to such a discrepancy is their large excitation energies, i.e. they have Q values significantly more negative than the lower-T states. Evidently DWBA calculations do not predict the proper dependence of cross-section on Q.

This is not too surprising. The prescription for obtaining the single particle bound-state wave function, or "form

factor", is to pick the well depth that binds the Lsj orbital with the right separation energy. But the data shows that pickup from the same orbital can lead to levels seven or eight MeV apart. To bind the particle with seven MeV greater separation energy requires a well ten MeV deeper. The particle is bound tighter, there is consequently less overlap in the transition amplitude integral, the predicted cross-section is too small and so the resulting spectroscopic factor is too large. While the simple shell model level scheme of Section 2.1 is known to be widely split by Coulomb or other residual interactions, each level is treated as a pure unperturbed single-particle level at the proper energy for the sake of the calculation.

One approach to this problem is to just ignore the change in binding energy. Sherr, et al., in their study of isobaric analog states in the titanium-nickel mass region (Sh 65) were able to improve agreement with predictions by using an "effective binding" procedure. In this scheme, the same bound-state wave function is used for all Q values, effectively ignoring the energy shifts caused by residual interactions. Unfortunately, this produces an incorrect exponential falloff outside the nucleus for the form factor, which the "separation energy" prescription is designed to produce correctly.

The use of a neutron bound-state wave function to represent the nuclear overlap is strictly correct only for pickup of a single particle outside a closed core (Pr 68). Thus, while the form of the overlap in the nuclear interior is open to

question, the exponential falloff outside is rather closely defined by the separation energy. Pinkston and Satchler, in an investigation of the Q-dependence problem (Pi 65), conclude that other features of the bound-state well must be changed, besides the depth, as a function of Q and that the effective binding procedure is essentially wrong.

Another manifestiation of the Q-dependence problem is the $^{48}Ti(p,d)^{47}Ti(G.S.)$ transition, which proceeds by a small $1f_{5/2}$ admixture. A well nearly ten MeV deeper than for the 0.16 MeV state is required to give the proper separation energy. The predicted spectroscopic factor is almost certainly too high. Prakash (Pr 68) has ameliorated this problem in (d,p) stripping by introducing "pseudopotentials", due to the presence of interacting extra-core nucleons, into the bound-state wave equation. Likewise Rost (Ro 67a) has developed a coupled-channels method for computing more realistic bound-state wave functions, for use in L= 3 transitions to analog states. The general problem, however, of properly reproducing Q-dependence in DWBA calculations is still a topic for discussion.

Thus, the results presented in Table 6.4 are of only limited reliability. Because in many cases spectroscopic factors are summed over a wide range of Q values, any systematic agreement with predictions can only be considered fortuitous. One can conclude, however, from the systematics of the (p,d) reaction over the titanium isotopes presented here, that the sum rule predictions presented in Chapter 2 are in good qualitative agreement with the data.

7. SPECTROSCOPY OF (p,t) REACTIONS

An investigation of (p,t) reactions in the titanium isotopes, paralleling the (p,d) studies, was conducted to gain additional information on isobaric analog states. For a target with non-zero T, three different final state T values can be reached via (p,t), as opposed to two for (p,d). Garvey and Bayman have suggested (Ga 64) that many (p,t) transitions to these highest-T states, having $T = T_z + 2$, should be enhanced over lower-T transitions of the same Q.

Using the MBZ wave functions and Coulomb systematics, they predicted the strengths and approximate Q values for (p,t) reactions on the even titanium isotopes and other targets. Shortly thereafter, Garvey, Cerny and Pehl (Ga 64a) published preliminary findings supporting the predictions, including a measurement of the T= 2 state in ^{44}Ti. Consequently it was decided to repeat this measurement and extend the search for $T_z + 2$ states to ^{46,48}Ti. Table 7.1 lists the predicted excitations and strengths, given in terms of the ground state strength.

Figure 7.1 shows a typical spectrum of ^{46}Ti(p,t)^{44}Ti at 39.24 MeV, indicating the levels observed and contaminants. Angular distributions for these levels are shown in Figure 7.2 and summarized in Table 7.2. The few spin assignments made are based on comparison with angular distributions of known levels (Ho 68) in ^{48}Ti(p,t)^{46}Ti measured at the same

Table 7.1 Predictions and results of $T = T_z + 2$ investigation.

Nucleus	Ex predicted	S/S(G.S.)	Ex observed	σ/σ(G.S.)
^{44}Ti	9.8 MeV	0.11	9.31 MeV	0.12
^{46}Ti	14.02	0.06	--	<0.03
^{48}Ti	16.8	0.04	--	<0.03

Table 7.2 Summary of results for ^{46}Ti(p,t)^{44}Ti at 39.24 MeV.

Ex (MeV)	σ_{lab}(mb/sr)	θ_{lab}(deg.)	T	J
0	0.50	22	0	0+
1.07	0.05	16		2+
2.87	0.05	16		(3-)
3.17	0.014	21		(4+)
3.36	0.008	25		
3.79	0.02	16		
4.01	0.04	15		
4.79	0.015	20		
5.05	0.01	25		
5.31	0.016	16		
6.03	0.01	26		
6.56	0.03	36		
6.90	0.03	16		
7.61	0.03	16		
7.88	0.01	26		
8.31	0.04	16		
8.68	0.04	16		
9.31	0.05a	25	2	0+

Note: a) Second maximum

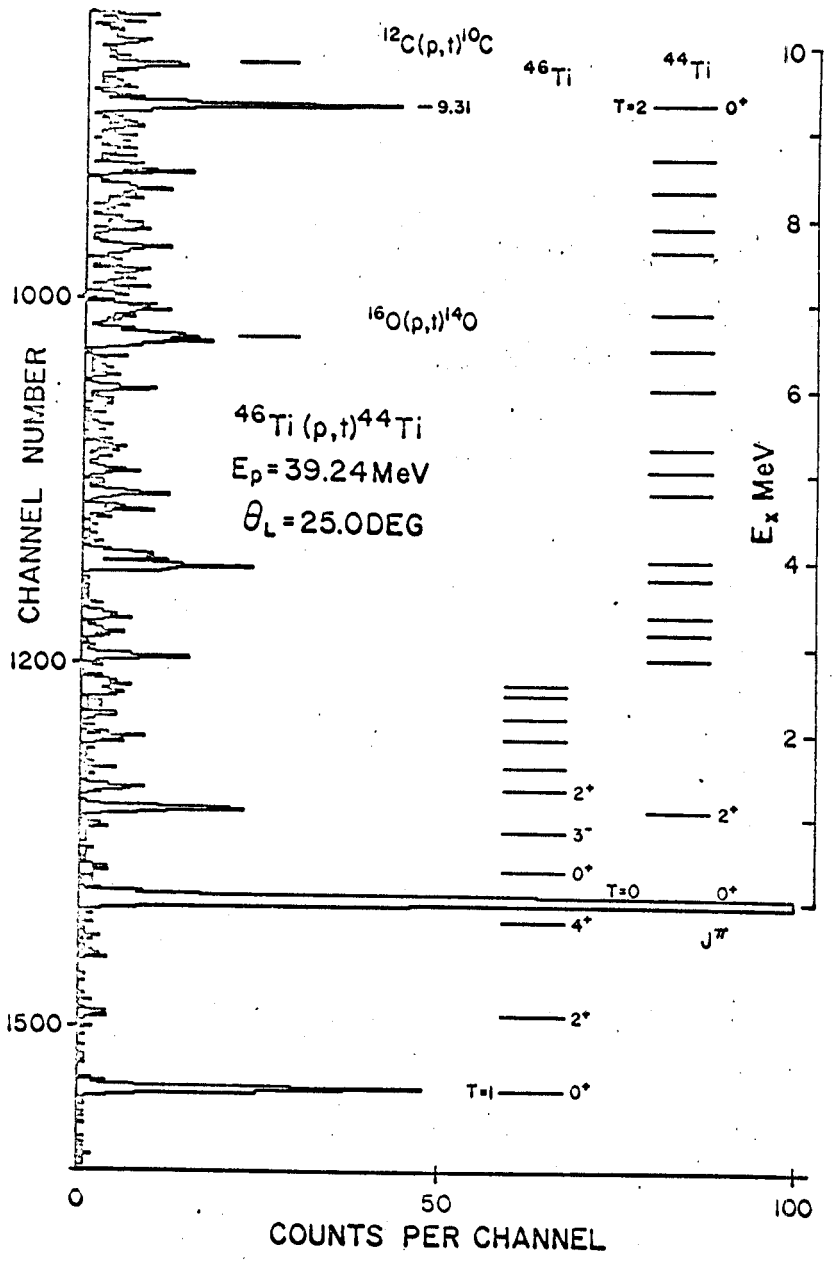

Figure 7.1 Triton spectrum from ^{46}Ti target and levels observed.

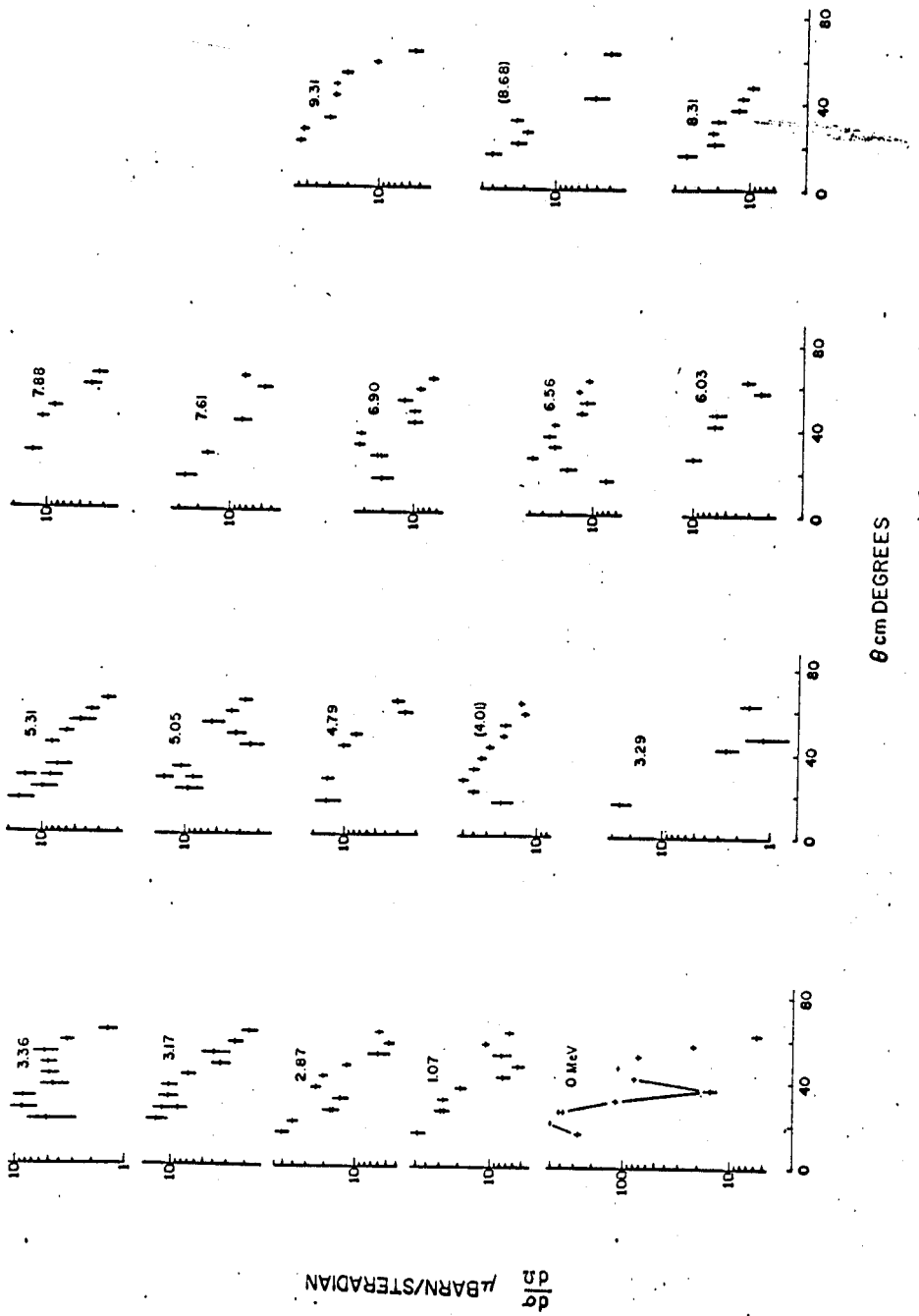

Figure 7.2 Measured angular distributions of $^{46}Ti(p,t)^{44}Ti$ at 39.24 MeV.

energy. Clearly, the 0+ level at 9.31 MeV is a prime candidate for being the analog to the ground state of ^{44}Ca. The T= 1 analog to ^{44}Sc is predicted to lie near 6.5 MeV (Sh 67), but there is no reason to expect it to be enhanced in (p,t) nor is there a nearby level definitely having the required 2+ spin. No assignment is made.

It was found that the published mass of ^{44}Ti (Mc 65) is too great by about 120 keV. An unusually good determination of the (p,t) Q value was possible in this study because the ^{44}Ti ground state is bracketed by states of well-established Q value in ^{46}Ti (Ho 68). Thus the ^{46}Ti(p,t)^{44}Ti ground state Q value was found to be -14.246(0.011) MeV.

Studies of the other titanium isotopes failed to locate the T_z + 2 analogs. The results of this search are listed in Table 7.1 alongside the predictions. Only the ratio of experimental cross-sections is given, rather than a ratio of spectroscopic factors, because of the many questions surrounding DWBA calculations for two-nucleon transfers (Pa 69). As can be seen from the table, however, the experimental ratio of cross-sections for ^{44}Ti is very similar to the predicted ratio of strengths. The upper bounds established for the other two reactions indicate that the levels should have been observed if the predictions are at all correct. A possible explanation is that these levels are split, since they represent configurations much more complex than ^{44}Ti. Even splitting into two approximately equal transitions could render them undetectable in this study.

LIST OF REFERENCES

An 69 S.A. Anderson, Ole Hansen and L. Vistisen, Nucl. Phys. A125 (1969) 65

Au 64 N. Austern, R.M. Drisko, E.C. Halbert and G.R. Satchler, Phys. Rev. 133 (1964) B3

Au 65 N. Austern, Phys. Rev. 137 (1965) B752

Ba 62 R.H. Bassel, R.M. Drisko and G.R. Satchler, Oak Ridge National Laboratory Technical Report ORNL-3240 (unpublished, 1962)

Ba 67 P.D. Barnes, J.R. Comfort, C.K. Bockelman, Ole Hansen and A. Sperduto, Phys. Rev. 159 (1967) 920

Ba 69 D.M. Bayer, Michigan State University Cyclotron Laboratory Sigma 7 Program Description 0013 (unpublished, 1969)

Be 64 T.A. Belote, E. Kashy, A. Sperduto, H.A. Enge and W.W. Buechner, Argonne National Laboratory Report ANL-6878 (unpublished, 1964) 109

Be 64a G. Bencze and J. Zimanyi, Phys. Lett. 9 (1964) 246

Be 65 T.A. Belote, W.E. Dorenbusch, Ole Hansen and J. Rapaport, Nucl. Phys. 73 (1965) 321

Bl 66 H.G. Blosser and A.I. Galonsky, IEEE Trans. on Nuclear Science, NS-B 4 (1966) 466

Bu 64 P.J.A. Buttle and L.J.B. Goldfarb, Proc. Phys. Soc. London 83 (1964) 701

de 63 A. de-Shalit and I. Talmi, Nuclear Shell Theory, Academic Press, New York (1963)

Di 65 J.K. Dickens, R.M. Drisko, F.G. Perey and G.R. Satchler, Phys. Lett. 15 (1965) 337

En 67 P.M. Endt and C. van der Leun, Nucl. Phys. A105 (1967) 1

Fr 61 J.B. French and M.H. Macfarlane, Nucl. Phys. 26 (1961) 168

Fr 65 M.P. Fricke and G.R. Satchler, Phys. Rev. 139 (1965) B567

Fr 66 J.M. Freeman, J.G. Jenkin and G. Murray, Phys. Lett. 22 (1966) 117

Fr 67 M.P. Fricke, E.E. Gross, B.J. Morton and A. Zucker, Phys. Rev. 156 (1967) 1207

Ga 64 G.T. Garvey and B.F. Bayman, Argonne National Laboratory Report ANL-6848 (unpublished, 1964) 125

Ga 64a G.T. Garvey, J. Cerney and R.H. Pehl, Phys. Rev. Lett. 12 (1964) 726

Gr 66 G.W. Greenlees and G.J. Pyle, Phys. Rev. 149 (1966) 836

Gr 67 A.M. Green, Phys. Lett. 24B (1967) 384

Ho 68 R.N. Horoshko, P.F. Hinrichsen and H.L. Scott, Nucl. Phys. A118 (1968) 609

Je 68 J.H. Jett, G.D. Jones and R.A. Ristinen, Phys. Lett. 28B (1968) 111

Jo 68 G.D. Jones, R.R. Johnson and J.H. Jett, Nucl. Phys. A111 (1968) 449

Ka 64 E. Kashy and T.W. Conlon, Phys. Rev. 135 (1964) B389

Ko 68 J.O. Kopf and P.J. Plauger, American Federation of Information Processing Societies 33 (1968) 1033

L'E 67 J. L'Ecuyer and C. St.-Pierre, Nucl. Phys. A100 (1967) 401

Le 67 L.L. Lee and J.P. Schiffer, Phys. Rev. 154 (1967) 1097

Lu 68 H.F. Lutz and T.S. Bohn, Nucl. Phys. A116 (1968) 112

Ma 65 J.H.E. Mattauch, W. Thiele and A.H. Wapstra, Nucl. Phys. 67 (1965) 1

Ma 67 G.H. Mackenzie, E. Kashy, M.M. Gordon and H.G. Blosser, IEEE Trans. on Nuclear Science, NS-14 3 (1967) 450

Mc 64 J.D. McCullen, B.F. Bayman and L. Zamick, Phys. Rev. 134 (1964) B515

Mc 64a J.D. McCullen, B.F. Bayman and L. Zamick, Princeton University Technical Report NYO-9891 (unpublished, 1964)

Mi 63 G.L. Miller and V. Radeka, Proc. NAS Conf. on Instrument Techniques in Nuclear Pulse Analysis, Monterey (1968)

Mo 60 R.H. Moore and R.K. Zeigler, Los Alamos Scientific Laboratory Report LA-2367, (unpublished, 1960)

Ne 67 E. Newman, L.C. Becker, B.M. Preedom and J.C. Hiebert, Nucl. Phys. A100 (1967) 225

Pa 69 R.A. Paddock, Ph.D. Thesis, Michigan State University, (unpublished, 1969)

Pe 63 C.M. Perey and F.G. Perey, Phys. Rev. 132 (1963) 755

Pe 63a F.G. Perey, Phys. Rev. 131 (1963) 745

Pe 64 F.G. Perey and D.S. Saxon, Phys. Lett. 10 (1964) 107

Pe 66 C.M. Perey and F.G. Perey, Phys. Rev. 152 (1966) 923

Pi 65 W.T. Pinkston and G.R. Satchler, Nucl. Phys. 72 (1965) 641

Pl 69 P.J. Plauger, Michigan State University Cyclotron Laboratory Sigma 7 Program Description 0010 (unpublished, 1969)

Pr 68 A. Prakash, Phys. Rev. Lett. 20 (1968) 864

Ra 66 J. Rapaport, A. Sperduto and W.W. Buechner, Phys. Rev. 143 (1966) 808

Ro 67 B. Rosner and D.J. Pullen, Phys. Lett. 24B (1967) 454

Ro 67a E. Rost, Phys. Rev. 154 (1967) 994

Sa 64 G.R. Satchler, Nucl. Phys. 55 (1964) 1

Sa 67 G.R. Satchler, Nucl. Phys. A92 (1967) 273

Sa 69 G.R. Satchler, description of Oak Ridge National Laboratory FORTRAN-IV computer code WAVDAM (private communication, 1969)

Sh 65 R. Sherr, B.F. Bayman, E. Rost, M.E. Rickey and C.G. Hoot, Phys. Rev. 139 (1965) B1272

Sh 67 R. Sherr, Phys. Lett. 24B (1967) 321

Sn 67 J.L. Snelgrove and E. Kashy, Nucl. Instr. Meth. 52 (1967) 153

Sn 68 J.L. Snelgrove, Ph.D. Thesis, Michigan State University (unpublished, 1968)

Sn 69 J.L. Snelgrove and E. Kashy, to be published in Phys. Rev. (1969)

Wi 66 C.F. Williamson, J.-P. Boujot and J. Picard, Rapport CEA-R 3042, Saclay (1966)

Wi 68 P. Wilhjelm, Ole Hansen, J.R. Comfort, C.K. Bockelman, P.D. Barnes and A. Sperduto, Phys. Rev. 166 (1968) 1121

Deuteron parameters used in previous (p,d) investigations (Ka 64, Sh 65) were taken from the 11 - 27 MeV study by Perey and Perey (Pe 63) which included no spin-orbit term. Most recent works include such a term, having the same geometry as the real well, and indicate that the real well depth should be approximately equal to the sum of typical proton and neutron depths (Pe 66). Thus, deuteron parameters for this thesis were estimated from (1) the 2.5 - 10 MeV set of Wilhjelm and Hansen (Wi 68), (2) the 11.8 and 21.4 MeV sets of Perey and Perey (Pe 66) and (3) the 34.4 MeV set of Newman, et al. (Ne 67).

Figure 4.1 shows the sample parameters and the choices made. The Wilhjelm set is plotted at 2.5 MeV where it gave the best fit. Extra weight was given here to the 20 - 35 MeV parameters, since most of the transitions studied produced deuterons of these energies. But since most energy dependence studies of optical parameter fits show no justification for varying anything but V, and since the more widely varying parameters seldom influenced the calculations strongly, all but V were taken to be independent of energy. The parameters used are also given in Table 4.2. Note that an imaginary volume term is not used.

Table 4.2 Deuteron optical model parameters.

V*	r_o	a	r_C	W_D
101 MeV	1.065 fm	0.81 fm	1.30 fm	10 MeV
r_{oI}	a_I	V_{so}	r_s	a_s
1.41 fm	0.75 fm	7 MeV	1.065 fm	0.81 fm

* V is given at 25 MeV. In general:

$$V = 117 - 0.627E_d \text{ MeV}$$

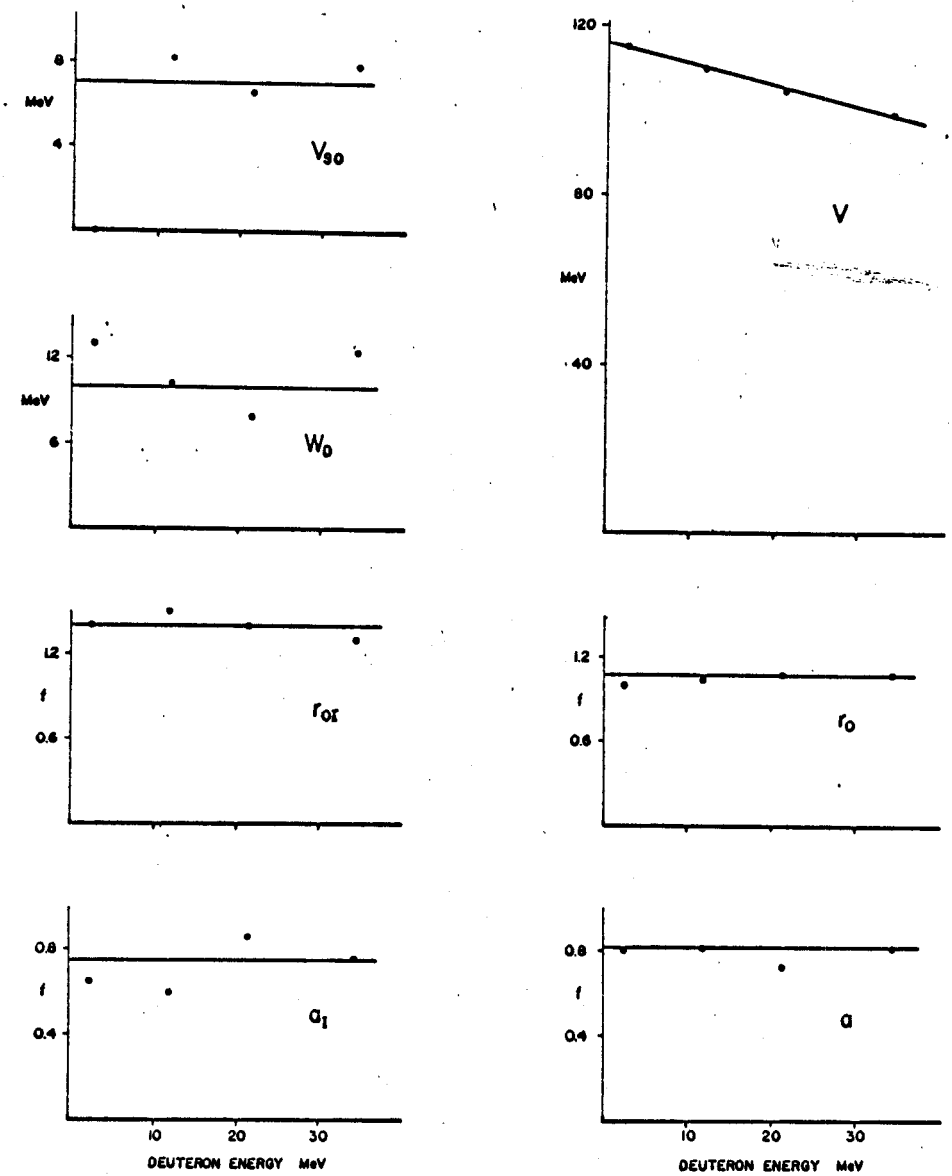

Figure 4.1 Deuteron optical model parameters.

To investigate the sensitivity of JULIE calculations to errors in the optical parameters, test cases were computed each with one of the parameters increased by ten per cent. Table 4.3 shows the results of this study for an L= 3 transfer at 25 MeV. The first three entries are for the neutron bound-state well, which employed the same (real) geometry used to describe elastic proton scattering. As expected, the dominant effects are caused by the real well depths and radii. The deuteron real parameters are surprisingly sensitive - a one per cent increase in radius causes a 4.7 per cent drop in peak cross-section (and a notable change in the shape of the cross-section). Care must be taken, therefore in interpreting absolute spectroscopic factors extracted.

Table 4.3 Per cent increase in peak (p,d) cross-section for ten per cent increase in parameter.

Parameter	Effect for p	Effect for d
r_o BSW	28 per cent	--
a_o BSW	8	--
r_C BSW	0	--
V	20	-47 per cent
r_o	20	-49
a	-2	5
r_C	0	-3
W	0	--
W_D	-2	-12
r_{oI}	-15	-21
a_I	-3	-17
V_{so}	0	0
r_s	0	--
a_s	0	--

5. ENERGY DEPENDENCE OF $^{48}Ti(p,d)^{47}Ti$

5.1 Experimental Results

Angular distributions of $^{48}Ti(p,d)^{47}Ti$ transitions have been measured over an angular range of eight to 90 degrees in the laboratory at 24.80, 29.82, 35.15, 39.97 and 45.05 MeV incident energies. Figure 5.1 shows a typical spectrum, aligned with the observed energy levels in ^{47}Ti. The L-transfer, J and T assignments for the strong transitions are taken from earlier studies (Ka 64, Sh 65, Ra 66, Ro 67).

Note that the principal transition occurs to the 0.16 MeV first excited state and not to the ground state. The latter is known to have spin 5/2-, and is expected to consist mostly of three $1f_{7/2}$ neutrons coupled to 5/2-. Since the direct pickup of a $1f_{7/2}$ neutron from a 0+ target cannot excite this state, the transition can only proceed in a direct process via $1f_{5/2}$ configuration admixtures in the target and final state wave functions. The 1f spin-orbit splitting is known to be on the order of 5.5 MeV in this mass region (Be 64) so the direct reaction cross-section for this channel is expected to be small (Be 65).

Thus the 0.16 MeV L= 3 transition is of prime importance in the energy dependence investigation. Also included in the study are the strong L= 1 transition at 1.54 MeV measured excitation and the L= 2 transfer at 1.81 MeV. The latter

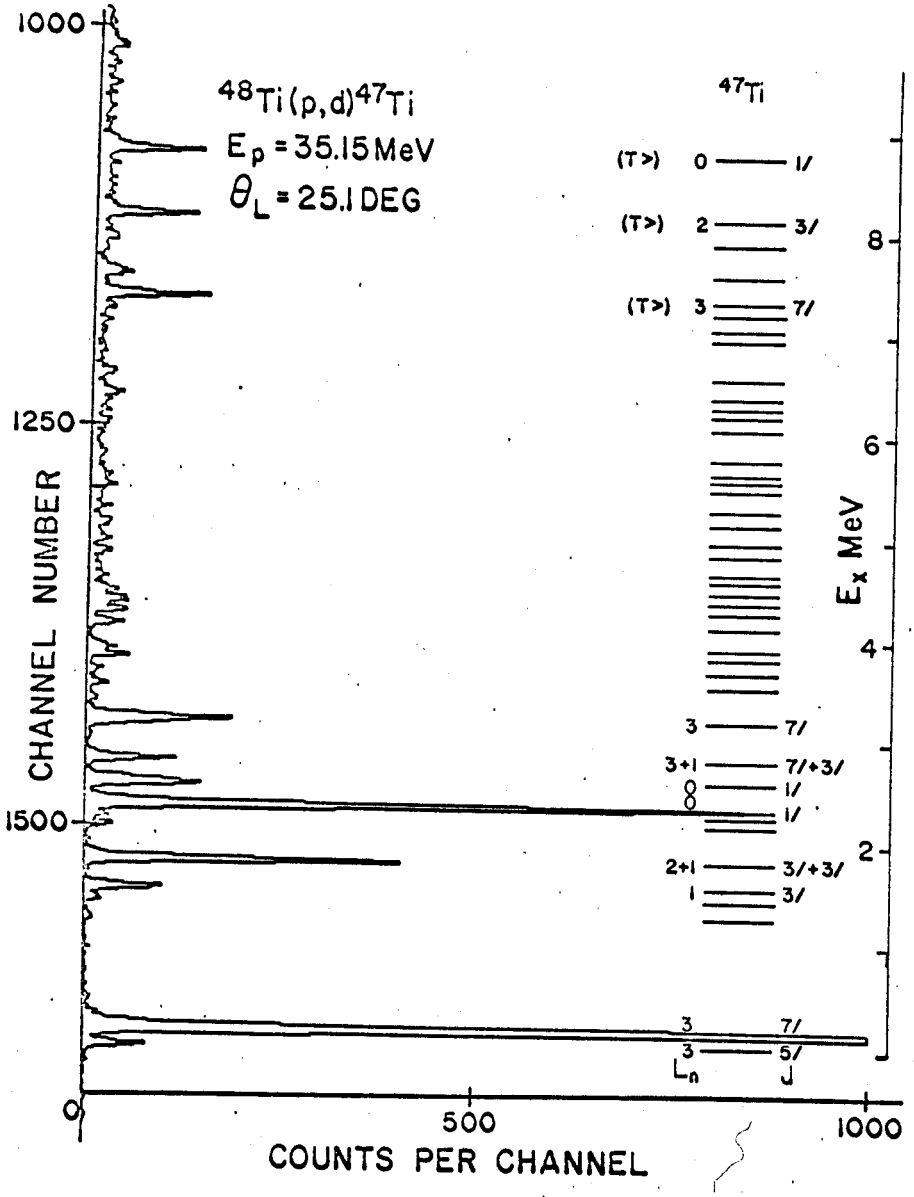

Figure 5.1 Deuteron spectrum from ^{48}Ti target and levels observed.

is known to be an unresolved doublet (Ra 66), which includes an L= 1 transition. This component is relatively weak, as will be shown later, and does not strongly influence the shape of the cross-section.

The three strong transitions between seven and nine MeV are to T= 5/2 analog states. One can locate such states by subtracting the n-p mass difference from the mass of the analogous state in ^{47}Sc, then adding the Coulomb energy required to bring an additional unit of charge into the nucleus. Systematics of Coulomb energies in this region have been investigated (Sh 67), and usually agree with observed analog excitations to within 100 keV. Analog state transitions stand out as concentrated deuteron groups against a nearly continuous background of states of lower T.

Above these analog states, in fact up to at least 20 MeV excitation, no significant transitions are observed. Thus one can characterize ^{48}Ti(p,d)^{47}Ti as leading principally to a few low-lying states in each isospin spectrum. Figures 5.2 and 5.3 show the odd-L and even-L transitions described above at the five incident energies. In addition, the strong L= 0 transfers measured at 2.35 and 8.74 MeV are displayed. Since these distributions are expected to have their principal maxima at zero degrees, they are not easily compared to calculated shapes and so play no role in the DWBA investigation.

All L= 3 cross-sections were found to increase quite

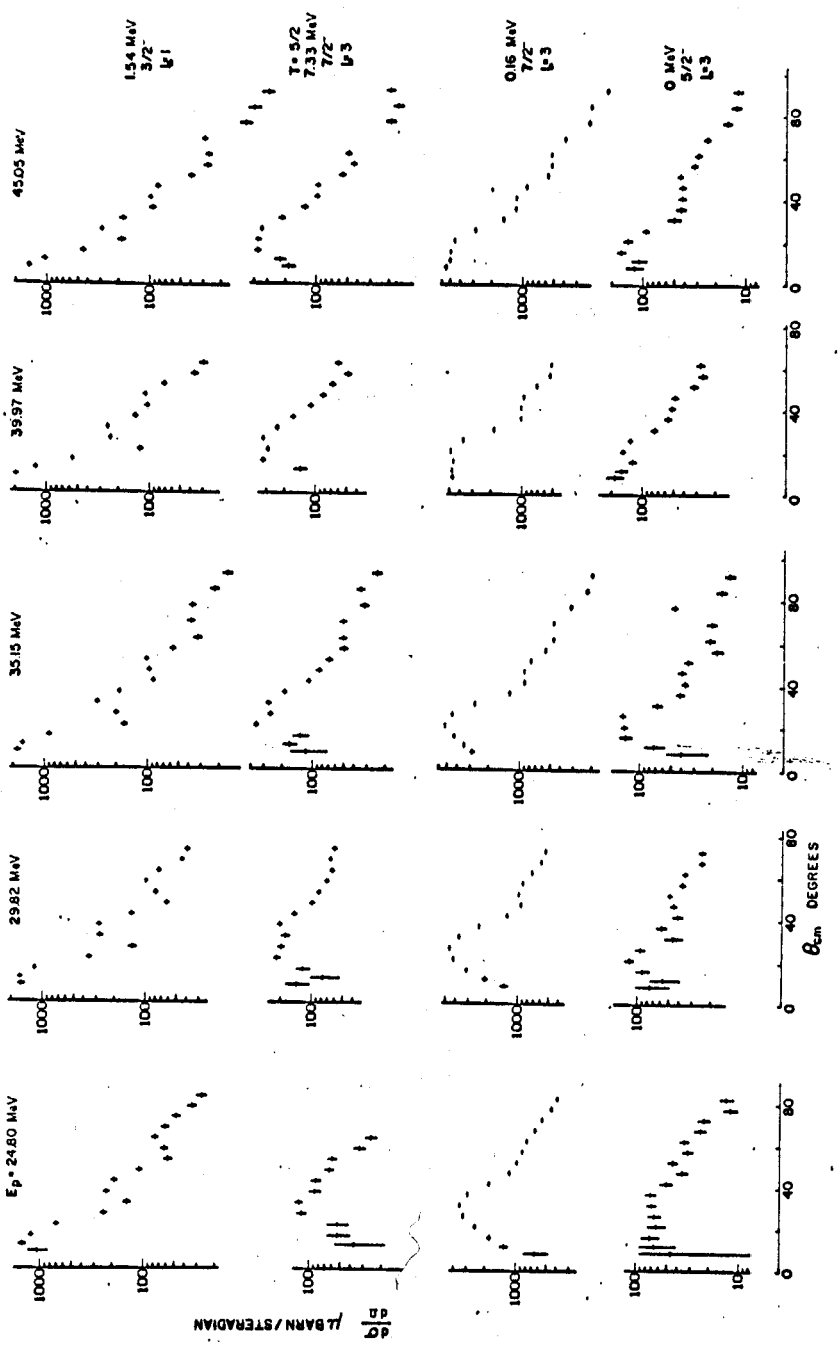

Figure 5.2 Energy dependence of odd-L transfers in $^{48}Ti(p,d)^{47}Ti$.